Lappeenranta University of Technology
Technical Faculty
Department of Energy Technology

Master's thesis

INTEGRATED ENERGY STORAGE TANK FOR LARGE SCALE POWER-TO-GAS APPLICATIONS

Examiners: Prof. Timo Hyppänen
D.Sc. Tero Tynjälä

Supervisors Doc. Pasi Vainikka
D.Sc. Vesa Tanskanen

Lappeenranta 20.5.2015

Hannu Karjunen

ABSTRACT

Lappeenranta University of Technology
Technical faculty
Department of Energy Technology

Author: Hannu Karjunen

Master's thesis: Integrated energy storage tank for large scale power-to-gas applications

Year:	2015	**Location:**	Lappeenranta, Finland
Pages:	99	**Figures:**	37
Tables:	7	**Appendices:**	0

Examiner:	Professor	Timo Hyppänen
	Doctor of Science	Tero Tynjälä
Supervisors:	Docent	Pasi Vainikka
	Doctor of Science	Vesa Tanskanen

Keywords: Energy storage, P2G, G2P, Power to gas, Liquefied Natural Gas, LNG, Computational Fluid Dynamics, CFD, Carbon Dioxide, CO2, Desublimation

The global interest towards renewable energy production such as wind and solar energy is increasing, which in turn calls for new energy storage concepts due to the larger share of intermittent energy production. Power-to-gas solutions can be utilized to convert surplus electricity to chemical energy which can be stored for extended periods of time. The energy storage concept explored in this thesis is an integrated energy storage tank connected to an oxy-fuel combustion plant. Using this approach, flue gases from the plant could be fed directly into the storage tank and later converted into synthetic natural gas by utilizing electrolysis-methanation route.

This work utilizes computational fluid dynamics to model the desublimation of carbon dioxide inside a storage tank containing cryogenic liquid, such as liquefied natural gas. Numerical modelling enables the evaluation of the transient flow patterns caused by the desublimation, as well as general fluid behaviour inside the tank. Based on simulations the stability of the cryogenic storage and the magnitude of the key parameters can be evaluated.

TIIVISTELMÄ

Lappeenrannan Teknillinen Yliopisto
Teknillinen Tiedekunta
Energiatekniikan osasto

Tekijä: Hannu Karjunen
Aihe: Integroitu energiavarastosäiliö suurille sähköstä kaasuksi –sovelluksille

Vuosi:	2015	**Paikka:**	Lappeenranta
Sivuja:	99	**Kuvia:**	37
Taulukoita:	7	**Liitteitä:**	0

Tarkastaja:	Professori	Timo Hyppänen
	Tutkijaopettaja	Tero Tynjälä
Ohjaajat:	Dosentti	Pasi Vainikka
	Tutkijatohtori	Vesa Tanskanen

Hakusanat: Energiavarasto, sähköstä kaasuksi, Nesteytetty maakaasu, LNG, Numeerinen virtauslaskenta, CFD, Hiilidioksidi, CO2, Härmistyminen

Maailmalla nouseva kiinnostus uusiutuvia energiamuotoja kohtaan kasvattaa tuuli- ja aurinkovoiman suhteellista osuutta energiantuotannosta, mikä puolestaan lisää tarvetta kehittää uusia energian varastointimuotoja tasaamaan vaihtelevaa sähköntuotantoa. Kaasumaiseen muotoon muunnettua sähköenergiaa voidaan säilöä kustannustehokkaasti pidempiäkin aikoja. Tässä työssä tutkitaan integroitua kaasuenergiavarastoa, joka on liitetty happipolttolaitokseen. Tällaisella ratkaisulla voimalaitoksen savukaasut voitaisiin ohjata suoraan varastosäiliöön, ja myöhempänä ajankohtana muuntaa synteettiseksi maakaasuksi elektrolyysi-metanointiprosessin kautta.

Tässä työssä käytetään numeerista virtauslaskentaa mallintamaan hiilidioksidin härmistymistä säiliössä, kun se on kosketuksissa kryogeenisen nesteen (kuten nesteytetyn maakaasun) kanssa. Numeerisen mallinnuksen avulla voidaan arvioida säiliössä härmistymisen johdosta syntyvää virtauskenttää sekä nesteen ja kaasujen yleistä käyttäytymistä. Simulaatioiden avulla voidaan arvioida tällaisen integroidun energiavaraston stabiiliutta, ja samalla saada käsitystä tärkeimpien parametrien suuruusluokasta.

ACKNOWLEDGEMENTS

This thesis was made in the facilities provided by VTT (Valtion tutkimuskeskus) and Lappeenranta University of Technology. Financially this project was made possible by the grant from Fortum Foundation. At this point I'd like to thank my supervisor, Pasi Vainikka for offering the subject and providing feedback, ideas and support throughout the process. I also express my deepest gratitude to Tero Tynjälä, Vesa Tanskanen Timo Hyppänen for all their guidance and efforts during the writing of this thesis. I'd also like to thank Ville Rintala and Jouni Hämäläinen for their contributions. Finally, a hearty thank you to my family and friends for their continuous support over the years. One can only be grateful for being surrounded by so many great people.

TABLE OF CONTENTS

Nomenclature

Latin letters

A	area	m^2
c	time relaxation coefficient	
c_p	specific heat capacity	J/kgK
F	force	N
f	face, drag function	
g	gravitational acceleration	m/s^2
H	height	m
h	specific enthalpy	J/kg
k	Turbulent kinetic energy	m^2/s^2
L	characteristic length	m
M	molar mass	kg/mol
m	mass	kg
n	mole	mol
P	power	W
p	pressure	Pa, bar
q	heat flux	W/m^2
q_i	lower heating value	J/kg
R	interaction force	N
S	source term	
T	temperature	K, °C
t	time	s
V	volume	m^3
v, w	velocity	m/s
x	vapour fraction	
Q	intensity of heat exchange	

Greek letters

α	thermal diffusivity	m^2/s
β	thermal expansion coefficient	1/K
ϵ	turbulent dissipation rate	m^2/s^3
ρ	density	kg/m^3
τ	particulate relaxation time	s
$\bar{\bar{\tau}}$	stress-strain tensor	
ϕ	property	

Subscripts

h	hydrostatic
l	liquid
lat	latent
p, q	phase index
sat	saturation
sen	sensible
th	thermal
v	vapour
vol	volume
vm	virtual mass

Abbreviations

BOG	Boil Off Gas
BOR	Boil Off Rate
CAPEX	Capital Expenditures
CC	Carbon Capture
CCS	Carbon Capture and Storage
CCU	Carbon Capture and Utilization
CFD	Computational Fluid Dynamics
CFL	Courant-Friedrichs-Lewy
CSP	Concentrated Solar Power
G2P	Gas-to-Power
LNG	Liquefied Natural Gas
LPG	Liquefied Petroleum Gas
MR	Multi-Refrigerant
NGL	Natural Gas Liquid
P2G	Power-to-gas
PCM	Phase Change Material
R&D	Research & Development
RES	Renewable Energy Source
RPT	Rapid Phase Transition
SMES	Superconducting Magnetic Energy Storage
SRK	Soave-Redlich-Kwong
UDF	User-Defined Function

Dimensionless numbers

C	Courant number
Gr	Grashof number
Re	Reynolds number

1 INTRODUCTION

With the increasing amount of intermittent renewable energy being added to the energy system globally, the demand for energy storage concepts is also on the rise. Gas-based energy storage concepts are generally based on converting electrical energy into chemical energy, which is stored in gaseous form. One of the largest benefits of such systems is that large scale storage is relatively cheap and easy to implement, as the technology is mature and readily available.

This thesis investigates a cryogenic tank capable of storing simultaneously liquefied hydrocarbons and solidified carbon dioxide. The term cryogenic refers to the low temperature state of the tank, typically around 110 Kelvin. If this type of tank is connected to an oxy-fuel combustion plant, it could potentially be used as a seasonal energy storage system. The working principle of such a storage in discharge mode would be that hydrocarbons are removed from the tank and combusted in an oxy-fuel combustion plant, and the resulting flue gases are then directed back into the same storage tank.

The benefit of using a single integrated tank over multiple storage tanks for different compounds is one of the important discussion points of this thesis. One potential benefit is the efficient transfer of latent heat between the substances: in a single tank the carbon dioxide would desublimate in direct contact with a cryogenic liquid. At a later time the stored carbon dioxide could be converted to synthetic natural gas by using an electrolysis-methanation process. The produced synthetic natural gas could then be combusted, which theoretically produces a closed loop for carbon.

1.1 Objectives

The objective of this thesis is to form a simple model capable of modelling carbon dioxide desublimation inside a storage tank. This developed model could be used to evaluate the possible issues and challenges that could be faced when carbon dioxide is desublimated in direct contact with a cryogenic liquid. The model is also a powerful tool in estimating the conditions inside the tank in various circumstances. Especially the evaluation of flow

behaviour inside the tank is taken as an important part of the model. Another important factor is the modelling of the boil-off phenomenon, which can be described as a surface evaporation process.

Based on the technology used in current liquefied natural gas (LNG) tanks, the overall feasibility of the described integrated energy storage tank is evaluated on a general level. The most critical phenomena connected to cryogenic storage are identified and discussed as well. If the development of this type of tank is continued, the discussion conducted in this thesis will be beneficial in identifying the key issues and focus points.

Initially, one of the objectives planned for this thesis was the evaluation of the possible thermal stratification inside the tank that could be induced by the carbon dioxide feeding. LNG tanks can be damaged by a phenomenon termed *rollover*, which is fundamentally caused by stratification inside the tank. However, the literature review conducted in this thesis showed that CFD models have not widely been used to predict the rollover phenomenon, and as such the focus of this thesis shifted more to other aspects of modelling. Also the literature review was extended in order to gain a better understanding of the state of research connected to cryogenic storage of liquids and desublimation. Another topic which was originally intended to be included in this thesis was the comparison of different types of feeding configurations for the carbon dioxide, but this was left out due to time restrictions.

1.2 Research method

This work uses computational fluid dynamics (CFD) software to simulate the behaviour of a tank containing liquefied methane. A transient two-dimensional axisymmetric CFD simulation of the tank is performed using ANSYS Fluent as the main simulation tool. The simulation uses an Eulerian multiphase model, which includes the gaseous and liquid phases of pure methane. Carbon dioxide feed-in process is modelled by implementing source terms for the momentum and energy in a specific location of the tank. With this approach, only two phases are modelled as physical materials, making the model less computationally expensive and simplifying the definition of simulation properties. In future studies carbon

dioxide could also be implemented as an actual substance. Material properties are mostly defined as constant values - with some exceptions: for instance density is in some cases defined by a real gas model.

The simulation is augmented by using user-defined functions (UDF) for various tasks. For instance, a UDF is used to implement an evaporation-condensation process at the liquid surface, giving an insight of the boil-off rate in the tank. Boundary values for the simulations are derived from literature, if possible. In some cases the boundary values are derived from general thermodynamic laws. Some aspects of this work can be considered to be on a concept level, which in this case means that some simulation values are based on educated guesses and approximations as no relevant literature references could be found or accessed.

1.3 Structure of the thesis

In the first chapter, some background information is given on the gas-based energy storage technology, and an overall status of the energy storage concepts is briefly introduced. Natural gas is closely connected to this subject, so the general properties and characteristics of natural gas are presented. Market status and future visions of the natural gas industry are also briefly discussed to give a general direction of the development.

The next chapter is about the different phenomena observed in natural gas industry and models describing them. LNG tanks are introduced, along with the important phenomena associated with cryogenic storage. A brief outlook is given on the different models used in the field of LNG tanks, after which the basics of the model developed in this thesis is introduced. Material properties, dimensions, boundary conditions and other important factors are derived in this chapter.

The fourth chapter is dedicated to the results from the simulations. First the issues encountered in the simulations are addressed, and later on some of the flow patterns are shown along with the evaluation of the boil-off model. Finally the conclusions of this thesis are presented.

2 POWER-TO-GAS

Power-to-gas (P2G) is a technology which is used to convert electricity into chemical energy. As an example, one can use electricity to decompose water via electrolysis, producing oxygen and hydrogen. The produced hydrogen could then be used in a fuel cell to produce electricity. Naturally, P2G technology is quite often closely connected to the reverse process, gas-to-power (G2P), as the previous example demonstrated. For simplicity, this paper will not make a distinction between P2G and G2P, so one can think that P2G also includes the reverse process in the context of this thesis.

In this chapter, the fundamental incentives for using and developing P2G technologies are introduced. The main working fluid is methane in this thesis, and because of the close resemblance of methane and LNG this chapter also gives an outlook on the natural gas industry and the basic principles in using liquefied natural gas. At the end of this chapter, the future and development of P2G technology is evaluated, along with a description of a novel concept of utilizing oxy-fuel combustion in conjugation with an integrated energy storage tank. In later chapters, the described energy storage tank is modelled using CFD.

2.1 Background

Renewable intermittent energy production has been raised as one of the driving factors for the need for increasing energy storage capacity [1]. The share of renewable energy sources (RES) will continue to increase in the European Union (EU), with current predictions of at least 55 % in gross final energy consumption by 2050 [2]. This large share of RES implies that significant investments need to be done in energy storage technologies to counterweight the large portion of intermittent energy production. Naturally, a wide geographical distribution of intermittent production, decentralized generation and smart grids somewhat alleviates the disequilibrium, but in the end grid balance will be dependent on adequate buffer and storage capabilities. [2, 3]

The potential demand for grid storage services has been predicted to increase from 3,2 GWh in 2012 to 185,4 GWh in 2017 globally [1]. The fundamental reason for storing energy is to

guarantee a secure supply of electric power and heat, and gas is one of the best candidates for the task as it is "abundant, available and affordable" [4]. As there is already existing infrastructure for gas-based technologies, the required investments are considerably lower than those required by other alternative technologies when evaluated on a larger scale. Gas-based technology can also be considered an already available relatively mature technology, which is something that cannot be said about large scale battery storages, for example. Another incentive for using gas-based technology is that in a shorter timescale gas could be used to substitute coal and oil to reduce greenhouse gas emissions. [2]

Currently energy storage capabilities in the EU are mainly in the form of pumped hydro-storage in mountainous areas. P2G technology offers another option for balancing electricity supply and demand in a timescale of roughly an hour or two. Also, due to the large existing natural gas network in Europe, P2G technology can be used to cover seasonal demand variations with low investment costs. However, one of the main issues in power regulation will be in a timescale of less than two hours, which represents the time between the unpredictable dropouts of solar and wind power, and the ramping up time of gas-fired boilers and other back-up plants. [5] P2G applications could potentially be used to cover this time period as well, since some systems are capable of dynamic operation [6]. P2G applications can therefore potentially tackle both the short and long term storage, which can be considered a unique characteristic among all the energy storage technologies.

Intermittent production of electricity commonly refers to solar and wind power, which are generally dependent on external factors such as weather. As can be seen from figure 1, Germany and Spain are the forerunners in the absolute amount of intermittent electricity production. As a comparison, figure 2 shows the relative amount of intermittent production (i.e. the share of intermittent production of the total gross electricity production). Germany and Spain have both exceeded the 10 % mark, while Denmark nearly reached 35 % in 2012. Current estimates state that a 20 % share of intermittent production is manageable in a modern power grid [1], although this is largely dependent on the performance and overall stability of the grid. This raises questions about the need of investing in additional storage capacity and improving interconnectivity in order to keep the electrical grid stable and operational.

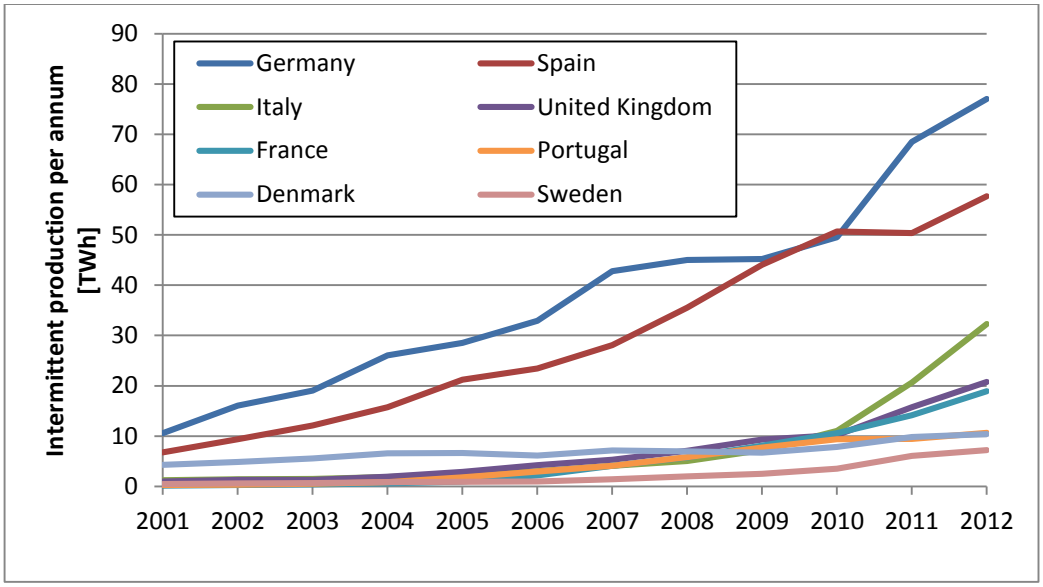

Figure 1. Intermittent (solar photovoltaic and wind power) electricity production in the EU. Only the top 8 countries are shown [7].

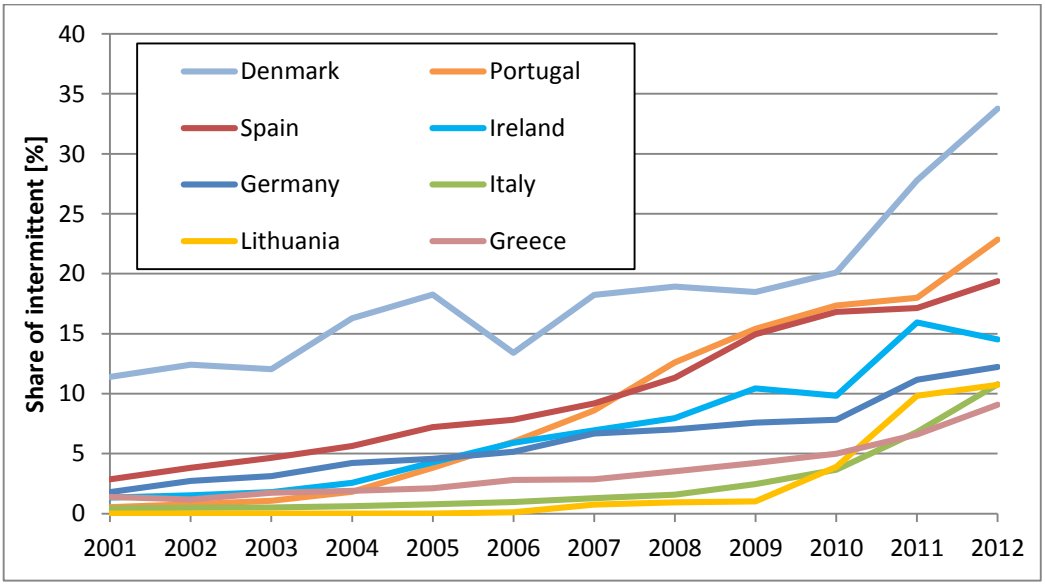

Figure 2. Intermittent production as a share of total gross electricity production. Only the top 8 countries are shown [7].

The increased amount of intermittent electricity production causes problems to conventional power plant systems, as the ramp-up time of these plants can be anywhere from a few hours to multiple days. Conventional power plants cannot dynamically follow the load demand, and as the renewable solar and wind energy replace electricity that was previously generated

in conventional power plants, full load hours of power plants decrease. This causes problems as typically the conventional plants have large investment costs and should be operated throughout the year with nominal load to yield maximum profit. The crisis between conventional power plants and intermittent power generation can already be seen in Germany's electricity prices, for example. There were 56 hours over 15 days in Germany which had negative electricity prices on the Day-Ahead market in 2012 [8]. Negative prices on the market can occur when there is a surplus of electricity production, and producers which operate inflexible facilities (such as nuclear power plants) choose to sell the generated electricity at a lower price rather than ramp down their production [9]. These negative prices reflect a potentially dangerous off-balance between the supply and demand of electricity, and actions need to be taken in order to guarantee stable electricity markets.

The fact is that power regulation will be a major factor in tomorrow's energy market, especially in areas which are heavily investing in renewable generation. The rapid increase of RES will cause grid instability that needs to be addressed in some way. Energy storage, in combination with improving grid interconnections, demand side load management, and the improving flexibility of power generating facilities are the most important tools in achieving this goal. New business paths could form around this subject, for instance in providing ramping services or stabilizing peak variations in the grid. To support this new development path there could be incentives through governmental legislation for boosting the energy storage businesses. [6]

2.2 Technology description

Power-to-gas is a process which converts electrical energy to chemical energy. The chemical energy is stored in the form of a gas, most commonly as hydrogen, methane or ammonia. This gas is ideally produced during times of low electricity demand and stored in tanks. This fuel could then be used later for example in a gas-fired boiler to produce electricity during peak demand hours. Figure 3 presents one possible utilization flowchart of P2G technology using either methane or hydrogen as the working fluid. The process begins with the production of hydrogen by decomposing water into its constituent elements in an electrolyser. After that, the produced hydrogen could be utilized directly, or it could be

processed into methane through methanation. A simplified flowchart of the process is presented in figure 4. The methanation process adds losses to the cycle, but on the other hand it produces methane which is already commonly used in various applications and therefore has existing infrastructure available.

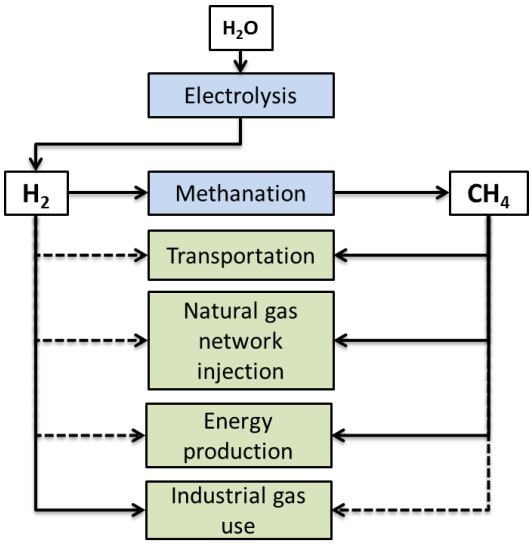

Figure 3. Different utilization paths for hydrogen and methane. Dashed lines indicate that the technology may not fully be considered as mature or profitable.

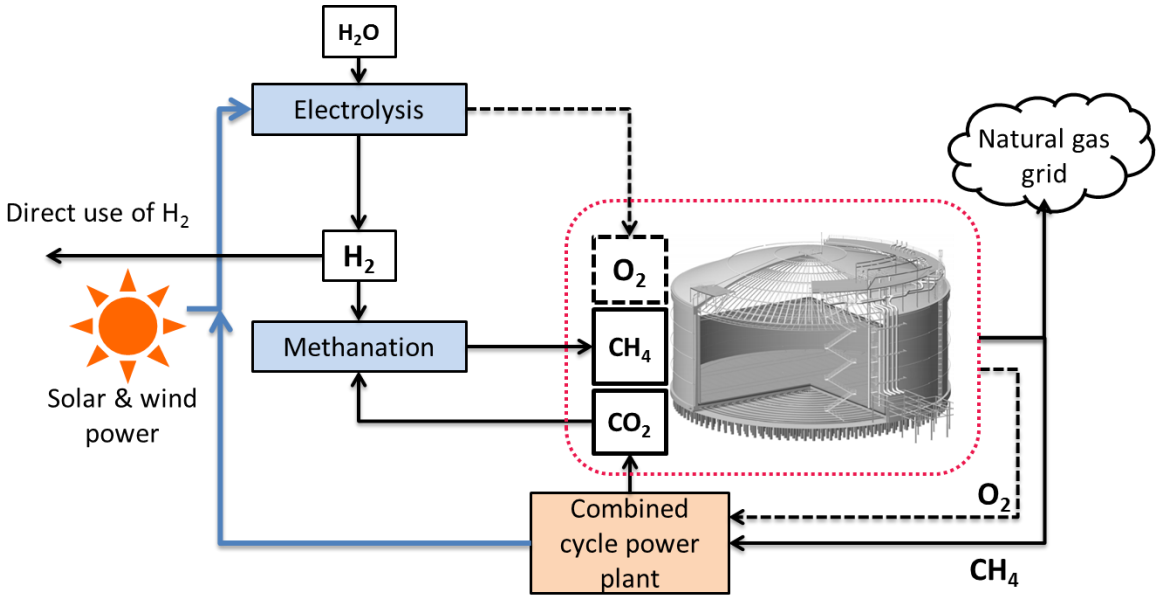

Figure 4. Flowchart of a P2G cycle process. Image of tank from [30].

Power-to-gas technology is best suited for large scale storage (>10 MW capacity), since no other energy storage technologies can achieve as low investment costs per a stored unit of energy while not being restricted by location [6]. Through the ongoing research and development (R&D) and increasing market, even small scale facilities could become profitable in the future. Seasonal storage is also possible through the utilization of large underground natural storage caverns or by using the existing natural gas network. Chemically stored components have a high energy density and minimal self-discharge, which is critical in long-term storage.

In small concentrations (less than 1-5 % [6], in some cases up to 15% of volume [10]), hydrogen produced with renewable sources could be added to the natural gas network to introduce a renewable component in the gas and reduce greenhouse gas emissions. Natural gas grid could also be used as a medium of transportation for hydrogen, but this concept would require significant investments in blending and extraction facilities, as well as a working infrastructure for efficient and rational use of hydrogen. Larger quantities and concentrations of the hydrogen are mainly restricted by the end-user requirements, material durability, and the costs associated with improving the grid to be suitable for higher concentrations. [10]

Another valid use for hydrogen is to use it as an ingredient in methanation, where the hydrogen and carbon dioxide (or monoxide) are combined to produce methane. This synthetically produced gas is comparable to natural gas, and it may be mixed with natural gas or used separately in same applications. [11] Common trade names for this product are substitute natural gas or synthetic natural gas (SNG). SNG can also be compressed or liquefied and used as a fuel in the transportation sector. There are also other alternative uses for the hydrogen besides the methanation route. Industrial chemicals, such as methanol, ethanol, ammonia, formic acid and urea could be produced by combining hydrogen with other compounds [6].

Environmental impact of the SNG is largely dependent on the source of carbon dioxide used in the methanation process. SNG can be produced from organic biomaterials, and the final product is quite similar as the one produced by methanation, but can vary slightly depending

on the employed technology. SNG produced from organic renewable materials is often abbreviated as bio-SNG, and the technology used to produce it is called *biogas upgrading*. The name refers to a process in which the gas is purified from contaminants, which also results in increased methane content. As a final product the purified gas is comparable to natural gas, and may be used in similar applications. Most common technologies for this process include water scrubbing, organic solvent scrubbing, amine scrubbing, pressure swing adsorption (PSA) and gas separation membranes. [12]

One of the most interesting future technologies is the integration of carbon capture into an oxyfuel combustion cycle using natural gas as a fuel. This technology potentially enables the recirculation of the captured carbon dioxide to be used in the production of methane. This concept has been discussed further in section 2.4. Naturally, the source of carbon dioxide is not restricted only to natural gas - in fact biogenic CO_2 could potentially have smaller environmental footprint when used this way. In conclusion, it can be said that natural gas industry and P2G applications offer a wide variety of different technological development paths, which is an asset in itself. There is always some uncertainty in predicting future predominant technologies, and the wide variety of available applications may be a crucial factor when the strategic technology development of individual companies are considered.

Drawbacks of the power-to-gas technology include the high capital expenditures (CAPEX) of the electrolysis unit [5]. Units with high CAPEX should optimally have high utilization period of maximum load i.e. maximum full load hours. Since the purpose of these power-to-gas units is to store energy in times of low energy demand, it restricts the operational time of the unit and thus lowers the overall economy. On the other hand, the rapid dynamic response of the electrolyser means that the technology could be effectively utilized in grid stabilisation purposes. Especially electrolysers which are based on the polymer electrolyte membrane (PEM) technology could prove to be useful in dynamic operation, although the technology is still under development and research. [6] One could also argue that the large costs of the electrolysers are likely to decrease significantly during the following decades as the technology develops and production quantities increase.

One further benefit of P2G technology is its capability to utilize existing natural gas infrastructure. Europe has a comprehensive natural gas network, LNG terminals could also be used in global trading, and natural caverns can be used for storage purposes. Currently the man-made natural gas storages in Europe have a combined capacity of around 97 000 million cubic meters (Mm^3) [13], which is by a rough approximation 20 % of the annual natural gas demand of 5000 TWh [14]. In addition there also exists nearly 128 000 Mm^3 of storage capacity in natural caverns. These storages are currently used as a buffer to cover the seasonal demand of natural gas. [15]

2.2.1 Alternative technologies

P2G technology is not the only contender in the energy storage business. A summary of different technological options is shown in figure 5.

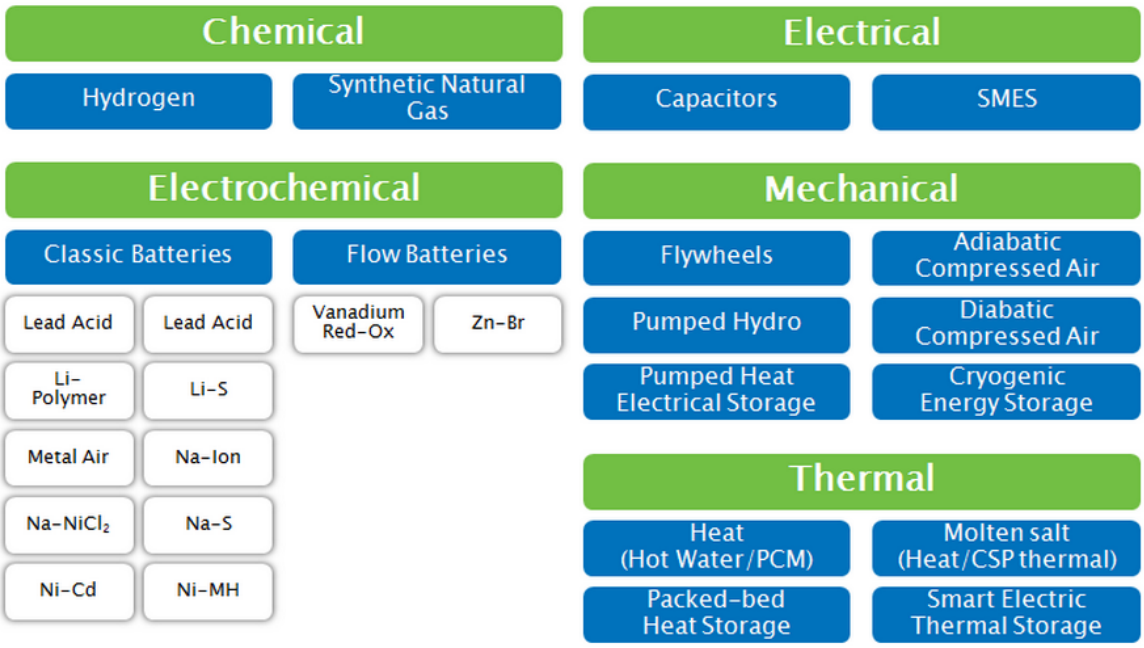

Figure 5. Energy storage options. Abbreviations used in the figure include superconducting magnetic energy storage (SMES), phase change material (PCM), concentrated solar power (CSP). [16]

Figure 6 describes the distribution of the different energy storage technologies according to number of projects in Europe. National projects are distinguished from projects funded by the European Commission. Electrochemical technologies are clearly being developed more vigorously, while pure electrical technologies (capacitors and SMES) only have a marginal

share. Chemical storage has a relatively good standing, followed closely by thermal and mechanical storages.

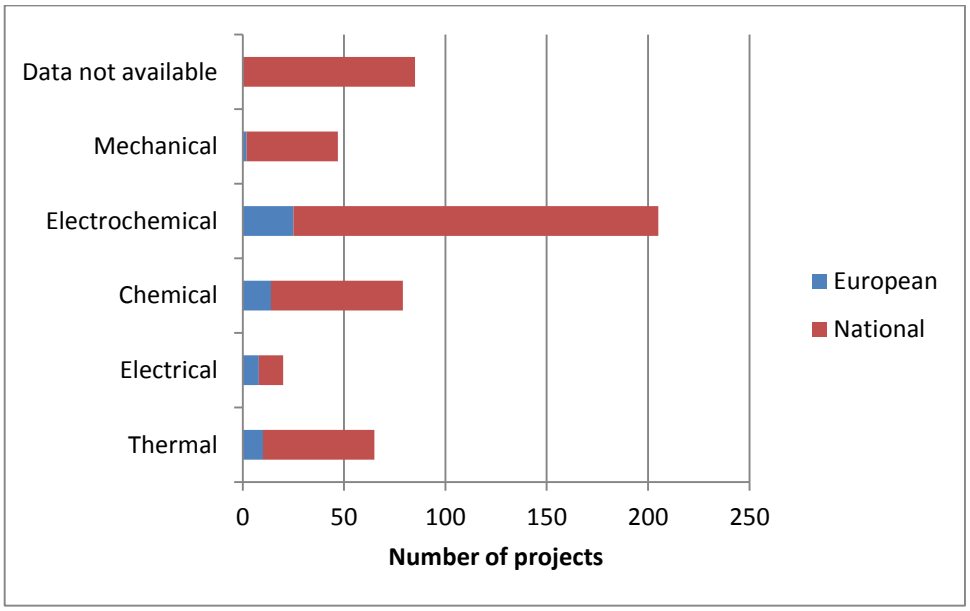

Figure 6. R&D projects among the different energy storage concepts in Europe. Projects distinguished between European and national funding. **[**3]

2.3 Natural gas

Oil has been the dominating fossil fuel on the market for decades. Oil is relatively cheap to transport, it has high energy density and international markets are well established. Economically natural gas is not competitive with oil, but environmentally it's superior to any other fossil fuel as natural gas has considerably lower carbon content per unit of energy. As such, the global interest in decreasing carbon dioxide emissions has established a foothold for natural gas in the energy industry [17].

Natural gas can be refrigerated to cryogenic temperatures (ca. 110 K), which causes the gas to liquefy at atmospheric pressure. Liquefied natural gas may then be stored in insulated tanks and later regasified for use. Liquefaction increases the density of natural gas about 600-fold [18], which is a large asset in transportation. The higher energy density of LNG makes its transportation in specially designed transport ships cost-effective, which enables the trading of natural gas internationally, and even on a global scale. Due to large increase in infrastructure and demand, the volume of gas traded between different regions is expected

to increase by 30 % between 2012 and 2018 [19]. Figure 7 shows a comparison of commonly used transportation fuels in terms of energy content per volume and per mass.

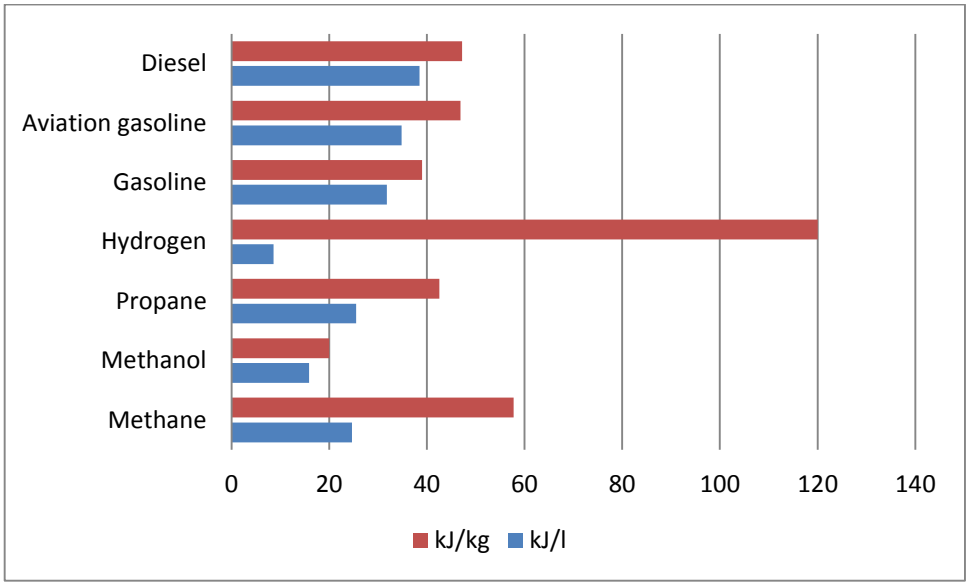

Figure 7. Energy content of transportation fuels per mass and volume. [20]

The composition and properties of LNG varies according to its source and degree of processing. Table 1 shows five different LNG compositions. It's beneficial to have the nitrogen content of the LNG below 1 % [18], as otherwise the excess nitrogen could cause unwanted phenomena such as rollover in the tank (see section 3.2 for details).

Table 1. Composition of LNG. [20]

Source of LNG	Methane	Ethane	Propane [mol%]	Butane	Nitrogen
Algeria	86.98	9.35	2.33	0.63	0.71
San Diego Gas & Electric	92	6	1	0	1
Baltimore Gas & Electric	93.32	4.65	0.84	0.18	1.01
Venezuelan	87.3	10.1	2.1	0.2	0.3
Alaska (Kenai)	99.72	0.06	0.005	0.005	0.2

2.3.1 Trends

Globally, natural gas industry is increasing rapidly in non-OECD countries, particularly in China with a 12 % growth rate per year. Africa, Middle East and Latin America are also

expected to experience high growth rates. Out of the OECD countries, America and Asia Oceania are the main drivers, whereas growth is estimated to be quite limited in Europe. [19]

There are a few globally interesting hot topics in the natural gas industry, which will have a significant impact on the liquefied natural gas market. As a brief summary, the most important topics are:

- shale gas production especially in USA and its export effects on the global markets, [21]
- increasing demand in the Asia pacific region and specifically the price competition between Europe and Asia,
- the role and competition of the large LNG export countries: United States, Australia, Russia, Africa and Qatar. [22, 19]

In the EU area, there is some interest to invest in the natural gas industry. These investments are primarily meant to secure the gas supply and improve natural gas source diversification [4]. Already during the last five years, Europe's gas infrastructure has become more secure due to increased storage capacity, LNG terminals and interconnections [23], and this development is ongoing as can be seen from the following figures. Figure 8 shows the cumulative installed storage capacity of LNG in artificial storages, as well as a projection for the future based on investment plans.

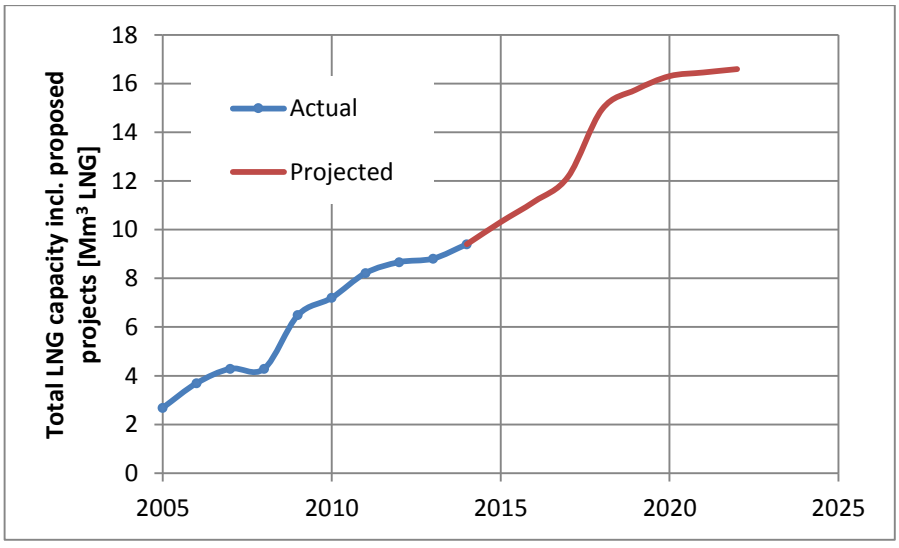

Figure 8. Actual and projected LNG terminal capacity in the EU [13].

Figure 9 presents the amount of currently open projects in the natural gas industry in EU projected in a ten-year plan and how they are distributed. Roughly 70 % of the investments are in pipeline development and other infrastructure, whereas LNG terminals and storage facilities respond for roughly 15 % each. The projects have been separated into final investment decision (FID) projects, and non-FID projects.

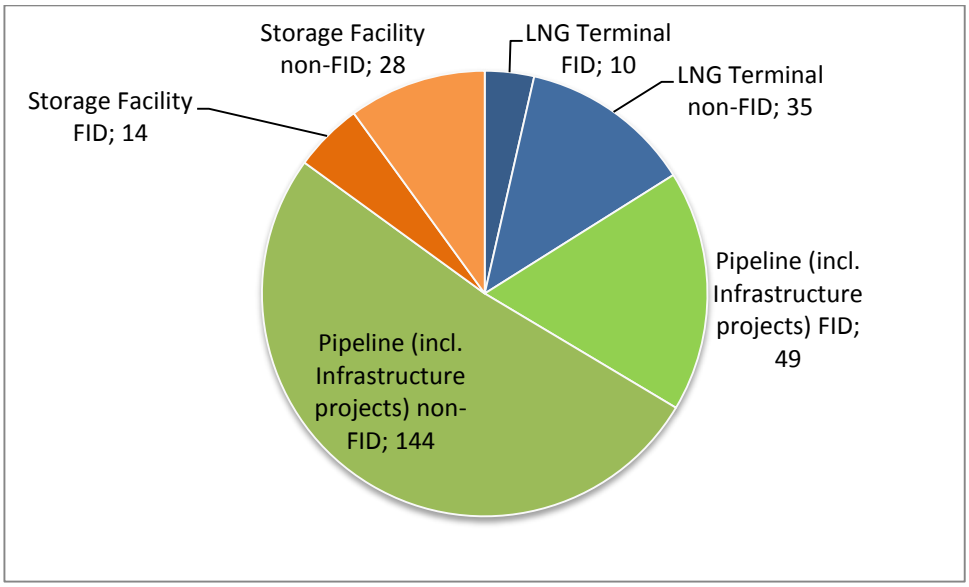

Figure 9. Number of natural gas projects in the EU in a 10-year development plan (2013-2022) [4].

2.3.2 Liquefaction and storage

Natural gas is liquefied in a facility complex called a *LNG train*, which consists of a refrigeration unit, a storage unit, and additional supporting facilities such as gas purification and marine loading systems for ship transport [17]. Figure 10 presents a typical flowchart through the liquefaction process.

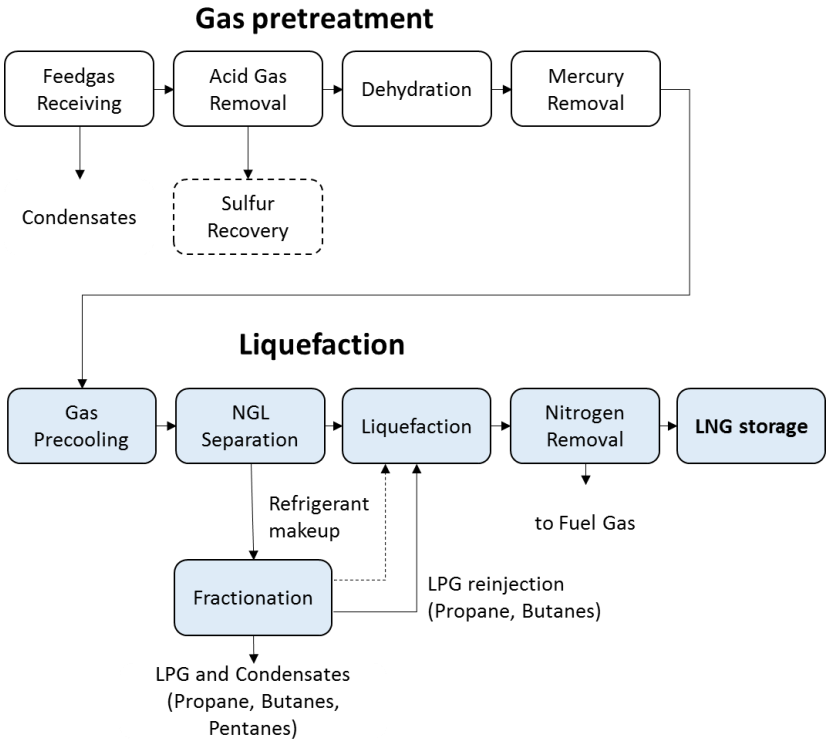

Figure 10. Flowchart of natural gas liquefaction process [17]. NGL stands for natural gas liquid and LPG for liquefied petroleum gas.

As a first step the natural gas is purified of substances that could cause complications further down the liquefaction process. One of the largest issues is the possible freezing of certain components within the heat exchangers. Acid gases, hydrogen sulphide, mercury, water and heavier hydrocarbons (pentanes, hexanes and aromatics) are removed. [17]

Liquefaction processes can be divided into pure refrigerant and mixed refrigerant (MR) processes. As the names suggests, pure refrigerants are composed of a single cooling substance, whereas MR processes may use, for instance, a mixture of hydrocarbons and nitrogen. Pure refrigerant processes may utilize a cascade process, which employs multiple pure refrigerants in separated stages at different pressure levels. This is more efficient than, for example, using a single component pure refrigerant like nitrogen in a single stage compression. [24] Some liquefaction processes are based on patented proprietary cooling fluids, which consist of a wide variety of chemical elements. Air Products & Chemicals Inc.'s Multi-Component Refrigerant (APCI MCR) is one of the most popular proprietary-refrigerant-based designs for natural gas liquefaction, with about 80 % of built LNG trains being based on this technology or its derivatives. [17]

2.4 P2G Development

Power-to-gas is at this point still under heavy research and development, and the full potential of many applications and technologies is yet to be unleashed. In this section, some of the most crucial issues and open questions are introduced, along with a brief description of oxy-fuel combustion, which is closely connected to the topic of this thesis.

Hydrogen is the cause for many issues with P2G technologies. Storage of hydrogen is problematic and even potentially dangerous, but there are some alternative solutions available. Firstly, it could be possible to store hydrogen in underground caverns, but this type of technology would only be interesting in a large-scale hydrogen economy. A more likely solution is that hydrogen is converted into other chemical components, such as ammonia or synthetic natural gas. These components are easier to storage than hydrogen, but on the other hand conversion losses decrease the efficiency. Once again this links to the future developments in storage technologies, which still have some room for development in pressurised operation, optimization, temperature control and electrical integration.

As stated previously, current electrolysers have a high CAPEX cost, which is one of the limiting reasons for the widespread use of P2G. Through R&D and economy of scale, the cost of electrolysers and linked components is likely to decrease in the future. With decreasing cost, the competitiveness of them is likely to increase between different technological concepts. Considering the electrolysers, there are two separate development paths: high- and low-temperature electrolysers. High-temperature electrolysers have good efficiency, but lack in the dynamic operation, whereas low temperature electrolysers have a good dynamic response but also a lower efficiency. There could be two separate markets for these types of electrolysers, one for steady state full load operation and one for dynamic operation. The dynamic operation could be intended, for example, to provide grid frequency control services. [6]

2.4.1 Oxy-fuel combustion and integrated storage concept

Oxy-fuel combustion refers to a process in which an oxygen-rich gas is used to feed a combustion process, instead of the traditional nitrogen-rich air. The resulting flue gases from the oxy-fuel combustion primarily consist of carbon dioxide and water, and depending on the fuel used a variable amount of SO_x and NO_x and other particles. [25] After an adequate purification process and dehydration, it is possible to store the flue gases, for instance in underground caverns or depleted oil reservoirs. It has been estimated that oxy-fuel combustion is the most cost efficient carbon capture (CC) technology, which is mainly credited to the larger boiler efficiency and minimal requirements for flue gas cleaning. [25] CC in natural gas fired power plants is a well-researched subject, and for instance Kvamsdal et. al. [26] gives a comparison on nine different cycles, six of which are based on the oxy-fuel combustion.

Alongside the traditional carbon capture and storage (CCS) theme, an alternative development path termed carbon capture and utilization (CCU) has received attention especially in Germany [27]. CCU is more focused on the efficient utilization of CO_2 in other processes, rather than in the long-term storage.

The novel concept investigated in this thesis is the utilization of a cryogenic storage tank to contain both the fuel and flue gases in the same vessel. The investigated vessel resembles a typical tank used for storing LNG. As stated previously, the flue gases from oxy-fuel combustion are relatively easily purified and after that stored, especially if the combustion fuel is composed of pure methane. Therefore, the stored carbon dioxide could then be used in a methanation process to produce synthetic natural gas, which could once again be used as a fuel in an oxy-fuel combustion process. In other words, this approach potentially offers a closed loop for carbon, with an added possibility of utilizing excess renewable electricity production to recirculate the carbon dioxide into synthetic natural gas during times of low electricity demand. Since natural gas is commonly stored in liquid form, cryogenic refrigeration equipment is likely to be available on-site, and this offers an excellent opportunity to potentially integrate cryogenic flue gas cleaning, natural gas liquefaction, as well as the storage of carbon dioxide and oxygen.

As a rough overview of the process, liquid methane would be vaporized from the tank and used in a combustion process. The resulting flue gases would be processed and passed through a heat exchanger. Finally the flue gases, which would at this point be nearly pure carbon dioxide, could be injected into the same storage tank as the liquid methane. Inside the tank the carbon dioxide would sublimate and cause some amount of liquid methane to evaporate. The evaporated methane could once again be combusted or utilized elsewhere. The previously mentioned heat exchanger could be, for example, used to vaporize oxygen, which has been stored in liquid or solid form in a separate storage.

However, the described process has many technical difficulties and open questions. First and foremost, mass and energy balances need to be considered and matched. In the best-case scenario, the amount of energy brought into the tank with carbon dioxide would be just enough to evaporate the required amount of methane in order to keep the power plant running at a steady power level. Additionally, the energy extracted from the flue gases would be enough to vaporize an adequate amount of oxygen so that the combustion process can continue. In a realistic situation, it's likely that some portion of the mass and energy needs to be directed out of the loop, by for example feeding excess boil-off methane to natural gas grid. Additionally the process will likely require some form of power input, as well as the regular addition of raw materials such as methane.

Technical aspects also pose a significant challenge. One of the biggest obstacles is the design of the thermal cycle. The pressure and temperature levels of the different compounds need to be matched with each other so that minimal amount of resources is lost between the phase changes and other reactions. In addition, it should be investigated whether a direct heat transfer method could be achieved through physical contact, or if a heat exchanger is required. The processing and handling of solid matter could also pose further challenges. Cryogenic temperature range also restricts the available construction materials, and the chemical reactions of the different elements need to be considered when evaluating material safety aspects. The previous listing of topics is by no means a complete survey, but rather a quick outlook in the most pressing matters.

3 MODELLING OF LNG STORAGE TANKS

The most compact method of storing and transporting gases is through a liquefaction process. Cryogenic storage tanks that are capable of storing liquefied gases have many unique characteristics from an engineering viewpoint when compared to heavily pressurised storage vessels operating at ambient temperatures. It is therefore important to understand some basic principles of cryogenic engineering before introducing different numerical models.

In the beginning of this chapter, a brief introduction is given on the technical details of a typical onshore LNG tank, as well as the most important phenomena associated with LNG and its storage. After that, a short summary is given on the status of the different computational and numerical models that have been utilized to model LNG tanks and other connected phenomena. Finally, the model used in this thesis is introduced. The developed model has been prioritised to evaluate the boil-off gas formation and fluid movement caused by the feed-in process of carbon dioxide.

3.1 Technical details

LNG is stored in large tanks which usually operate at a temperature region of -160 °C if the tank is not pressurised. Naturally, the operating temperature is dependent on the pressure inside the storage vessel, and for instance a pressure of 6 bars increases the operating temperature to roughly -135 °C. [28] The composition of the LNG also affects to the operation temperature. Tanks contain natural gas in both liquid and vapour phases, and constantly a portion of the liquid evaporates due to heat leaks into the tank from the surroundings.

Cryogenically stored liquids require a thermally insulated storage vessel or tank to minimize the dissipation of the substance. Large scale LNG storage tanks are typically flat bottom cylindrical vessels operated at ambient pressure, whereas tanks used in transportation are often spherical or horizontally aligned cylinders with hemispherical heads. Pressure in the

transportation vessels is usually in the region of a few bars above the ambient pressure [29]. Pressurised vessels are not investigated further in this thesis.

Typical storage volume of a large scale onshore LNG storage tank is in the range of 50 000 – 150 000 m^3 [13], but tanks up to 200 000 m^3 have been built [30]. Dimensions of such a tank are quite massive. For instance, a LNG tank in Cartagena, Spain with a storage capacity of 150 000 m^3 has an outer diameter of 81 m and a height of 40m [31]. For this thesis, a moderate tank size of 78 500 m^3 storage capacity was chosen, with an inner tank diameter of 50 m and a height of 40 m.

Figure 11 shows a view from the inside of an LNG tank during a hydro test. LNG inlet pipes and measurement devices can be seen near the tank walls. With careful observation also the holes for pressure relief valves on the tank roof are visible.

Figure 11. View from inside a LNG tank during a hydro test. [32]

EU standards that cover LNG storage tanks are EN 14620 and EN 1473. Storage tanks with a smaller capacity of 5 – 200 tons are covered by EN 13645. In addition, the standard EN 1160 covers some general characteristics of LNG. The introduced standards dictate for instance, that the tanks need to have a safe mechanism for removing boil off gas from the tank, and that the rate of heat leak into the tank should be minimized. One should note that pipe penetrations of the primary or secondary container base or walls are prohibited, which means that the only allowed route for pipe connections are through the roof. This also means that the pumps need to be submerged, and maintenance operations require suitable lifting equipment. [33]

3.1.1 Tank types

Tanks can be single containment, double containment or full containment tanks. A single containment LNG tank consists of an inner tank which is in contact with the LNG, and an outer container, which acts primarily as a protective shell for the inner tank and as a support structure for the insulation. If a significant leak occurs, the outer tank will collapse as the material is not designed to withstand cryogenic temperatures. Therefore single containment tanks require an external bund wall or dyke to capture the spilled liquid. [29]

In a double containment LNG tank, both the inner and outer tank are capable of independently containing the refrigerated liquid. It is, however, not designed to capture any vapour resulting from a leak. A full containment is also fitted with the ability to capture and vent the vapour in a controlled fashion from the tanks. [29] Figure 12 presents a simple flow diagram for determining the type of a container.

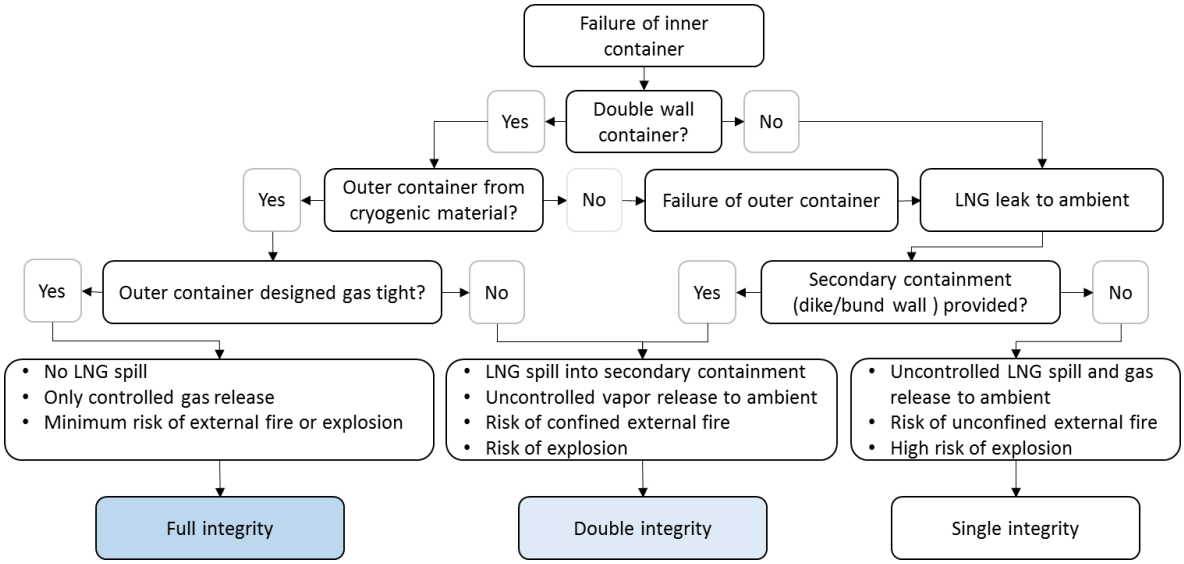

Figure 12. Flowchart for determining tank integrity type. [29]

3.1.2 Materials

There are a few suitable materials for the containment of LNG at cryogenic temperatures. One of them is a 9 % nickel steel alloy, which was introduced in 1946. It became more or less a standard material for cryogenics after outperforming other materials in a test called *Operation Cryogenics* in 1960, which involved hurling a two-ton wrecking ball from the height of about 6 meters against a vessel cooled to -195.6 °C [34]. Alternative materials include other austenitic stainless steels, 36 % nickel steel (Invar) and aluminium alloys. Recently, steels with a nickel content of 6-7 % have been commercialized in LNG tanks. [35, 36]

The key specifications cryogenic materials have to fulfil are low thermal conductivity, high strength and high stiffness [37]. A common structural problem with cryogenic materials is a sudden failure termed as *zip-failure*, which occurs due to material brittleness caused by the cryogenic temperatures weakening the material. [38]

The research and development of low-temperature materials has increased in 30 years, but mainly in the field of superconductors. Structural metal and alloy research has increased in Asia, but elsewhere in the world the trend is in decline. [39]

Typically, in the case of single-containment tanks, the inner tank is made of 9 % nickel, outer tank is carbon steel and insulation material is perlite. Double containment has similar inner structure, but the outer tank is prestressed reinforced concrete or other reinforced concrete. Full containment tanks also have a concrete roof for vapour-proof construction. Single-containment tanks require a larger surface area because of the dyke, but double containment tanks are about 40 % more expensive. Full containment tanks cost about 50 % more than single containment tanks. [17]

3.1.3 Heat transfer and flow patterns

As a LNG tank is kept at cryogenic temperatures, heat leaks from the ambient environment are significant. Insulation reduces the heat leaks, but still the liquid is constantly being heated by the heat leaks through the container walls. Major heat flows are through the wetted area of the inner container. Nucleate boiling does not occur, since the heat flux is too small, but the temperature differences arouse buoyancy-driven flows. [39]

LNG tanks have a heating system beneath the tank to maintain the soil above freezing temperature. This eliminates the possibility of frost heaving and the formation of ice lenses beneath the tank. [40, 41] Inevitably, this also increases the amount of heat leak through the tank flooring.

As to the flow patterns in the tank, a high-velocity flow develops on the vertical walls of the container, which transports heat from the lower parts of the tank to the surface. Fluid in contact with the tank floor is swept along to the edges of the tank where it joins the vertical flow. At the surface, the flow begins to move radially inwards while evaporating at the same time. Once the flow reaches the centre of the tank, it turns downwards and travels towards the core of the tank, where it mixes with the bulk liquid through a series of secondary flows. As stated before, there is no aggressive boiling or nucleate boiling inside the tank, but rather a buoyancy-driven flow to the surface and an evaporation process on the liquid-vapour interface. [39]

Modern cryogenic storage tanks utilize a technique called *vapour cooling*, which is used to absorb heat in-leaks. When a fluid at saturated temperature absorbs thermal energy, it is

absorbed by the *latent* heat of evaporation, causing the liquid to evaporate. The temperature of the evaporated fluid subsequently increases if it is heated further, in which case the heat is absorbed as the *sensible* heat of the vapour. Vapour cooling refers especially to the utilizing of the sensible heat to reduce the amount of liquid vaporization, by for example, introducing a counter current flow into a tube to absorb the heat in-leak. Another similar structure is a radiation shield, which is widely used in large LNG tanks to reduce the boil-off rate. The construction consists of a large plate, which absorbs the radiation in the upper part of the tank while simultaneously being cooled by the convective flows of the vaporized natural gas. [39]

Perlite is commonly used as an insulation material due to its low price. Other insulation methods, such as vacuum insulation or multilayer insulation (MLI) are technically better, but the economic costs often overrule their usage in large scale storage tanks. [38] Perlite can be categorized as a powder insulator. Powders aim to minimize the convective heat transfer by providing small gas voids, as well as reducing radiation and inhibiting gas conduction. Common powder materials are perlite, colloidal silica and silica aerogel. Foams and fibre-based insulation methods are an alternative to powder insulation, and these form a low-density solid-gas mixture, which lowers the conductive heat transfer. [39]

3.2 Phenomena

There are a few important phenomena connected to the storage of liquefied natural gas. In the following sections terms such as boil-off, weathering, rollover and rapid phase transition are explained briefly. The understanding of these phenomena is critical when one deals with the modelling of LNG storage containers.

3.2.1 Boil-off

The boundary between the liquid surface and the vapour space exchange both heat and mass through an evaporation-condensation process, which is commonly termed *boil-off* in LNG tanks. The phenomenon is further complicated by the composition of the liquid, since it is a mixture of multiple hydrocarbons and nitrogen. Essentially the boil-off process is analogous to distillation, which means that the different compounds of the liquid have different rates

of evaporation. Thus the volatility of the compounds dictates the composition of the evaporated vapour and the remaining liquid. Figure 13 presents a schematic of a LNG tank, with heat leaks and boil-off generation described by arrows.

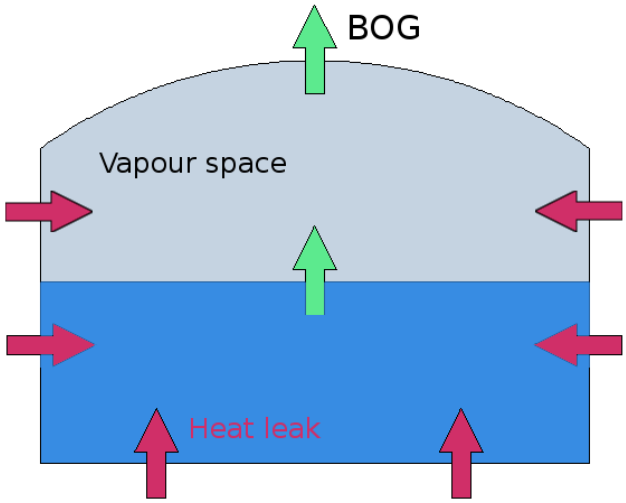

Figure 13. Schematic of a LNG tank. Heat leaks are described by red arrows, and mass transfer by green arrows.

LNG tanks operate at a gauge pressure of approximately 150 mbar [42]. The liquid in the tank is kept approximately at the same temperature by the constant evaporation of a portion of the LNG. Heat leaks into the tank cause slight temperature variations in the liquid, which in turn causes some buoyant mixing to happen in the tank. The evaporated vapour accumulates to the top section of the tank, and gradually the pressure inside the tank increases. LNG tanks are equipped with a pressure relief valve capable of removing the boil-off gas (BOG) from the tank [33], otherwise a pressure build-up could cause structural damage to the tank [43]. EN 1473 states that if the pressure relief valves are not designed to safely discharge BOG generation from a rollover, a rupture disk must be used. The purpose of this disk is to protect the integrity of the rest of the tank from over-pressure by temporarily sacrificing gas tightness. [33]

Since the tank pressure is dependent on the ambient pressure, weather can also have an effect on the boil-off rate (BOR): barometric highs cause the total pressure of the tank to increase and thus decrease the BOR and vice versa [42]. BOG can be re-liquefied, used as a fuel or injected into a gas network. Last resort options include flaring the gas or venting it to the atmosphere. [33]

Typical BOR of a LNG storage tank is about 0.05-0.1 % of LNG volume per day [38]. BOG composition is dependent upon the composition of both the LNG and the space which the LNG evaporates into. Typically the BOG composition is about 20 % nitrogen, 80 % methane and traces of ethane. It should be noted that the nitrogen content in the boil-off gas can be about 20 times larger than in the LNG, as nitrogen is more volatile than the hydrocarbons in LNG. [44]

3.2.2 Weathering

When LNG is stored for longer periods of time its composition changes slightly. This is termed *weathering*, and it is caused by the different vaporization rates of the LNG components: methane evaporates at a faster rate than the heavier hydrocarbons like ethane and propane. As the BOG is periodically removed from the vapour space, the density of the remaining liquid increases, which may be problematic when another batch of LNG is introduced into the same container. [42] Weathering can therefore contribute a phenomenon termed rollover, which is discussed next.

3.2.3 Rollover

Rollover is a phenomenon that may occur between stratified liquid layers. In the case of the LNG tanks, two stratified layers of LNG will rapidly mix and cause a large amount of BOG to be generated. The stratified layers are initially in different temperatures and densities, but heat and mass transfer between the liquid layers in combination with the heat-in-leak through the tank surfaces can cause the density differences to diminish. With similar densities, there is no acting force to prevent the mixing of the layers. Since the layers are not necessarily in the same temperature, different vapour pressures can cause a sudden increase in the boil-off rate. [45]

Rollover is most likely to occur when a new batch of LNG (called *cargo*) is inserted into a tank, because the properties of the existing liquid (called *heel*) are likely to be different. If the introduced cargo is lighter (as it often is) and inserted above the heel, two liquid layers form. Both layers would receive thermal energy from the heat leaks through the container walls, but the lower layer could heat up faster. [42] This results from the fact that up to 50 % of the heat leak is through the flooring [46]. Another reason for the faster heating of the

lower layer is the limited heat transfer through the layer interface, and also the constant evaporation at the topmost layer which drains thermal energy from the liquid surface. Figure 14 presents a schematic of a situation when two stratified layers are formed.

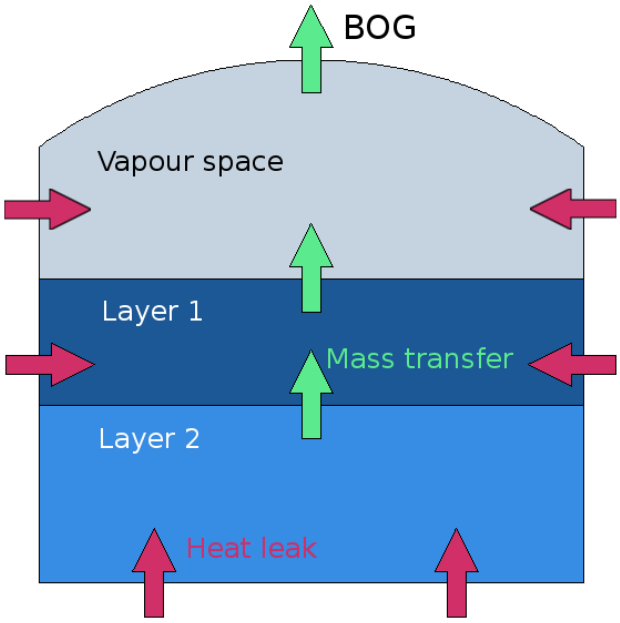

Figure 14. Schematic of a situation leading to a rollover.

The increasing average temperature in the lower layer causes the density to decrease. Simultaneously there is a mass transfer of heavier hydrocarbons from the heel to the cargo, which also affects the density balance of the different layers [47]. As the density difference between the layers is diminished, a rollover occurs.

The rollover phenomenon consists of two phases. First there is the slow and stable phase, which features a stationary interface. The interface is dominated by a double diffusive convective flow. Later on, as the density difference between the stratified layers decrease, penetrative convection becomes the dominant exchange mechanism at the interface. This type of flow features plumes of liquid which travel through the interface and eventually return due to buoyancy effects. This type of behaviour is characterised typical for the second phase of the rollover phenomenon. [42] Figure 15 presents the evolution of temperature and density in a tank containing two stratified layers.

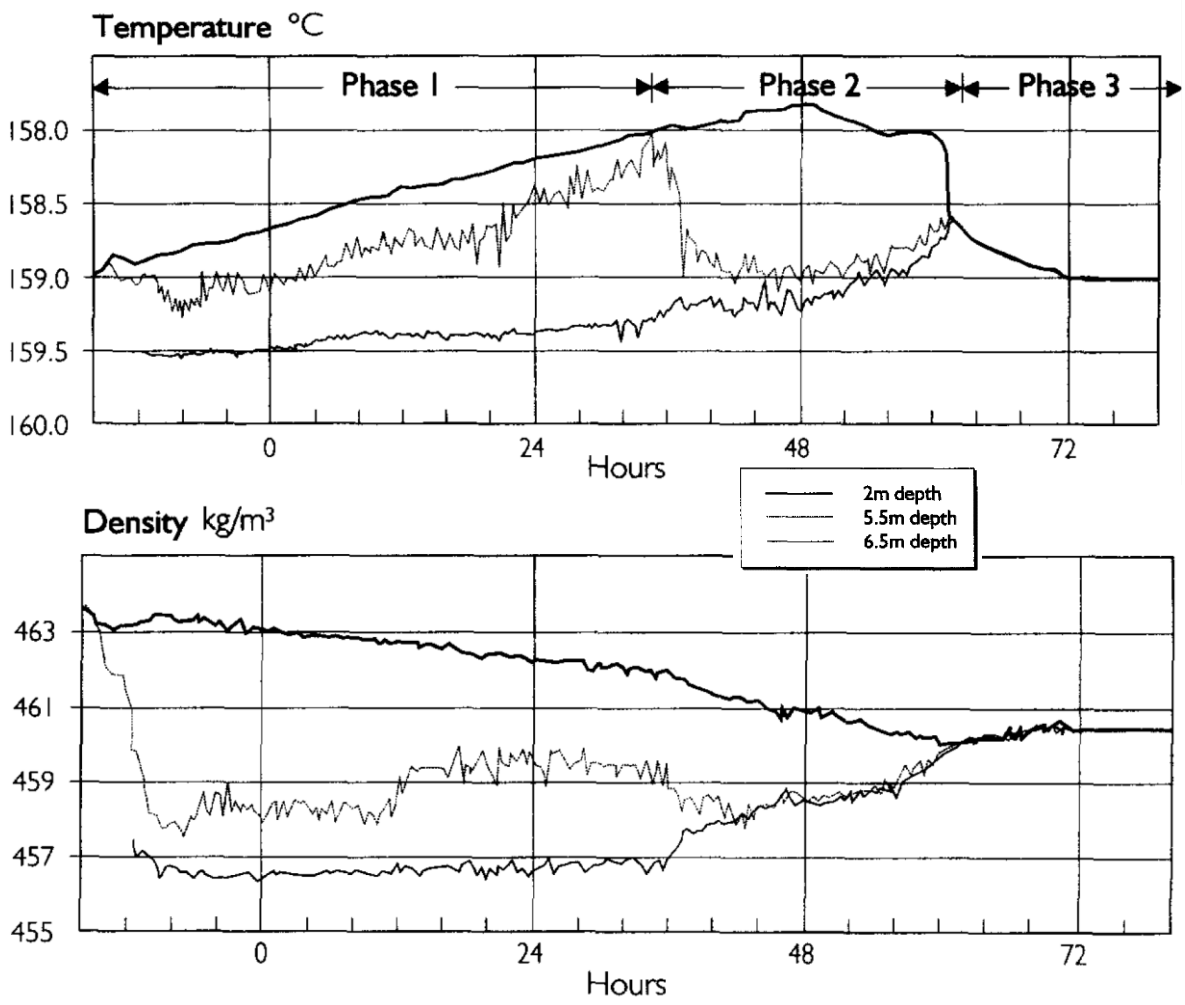

Figure 15. Evolution of temperature and density in a tank, measured from three depths. The phases 2 and 3 are the actual phases associated with the rollover phenomenon, and the first phase can be considered as a preliminary phase. [42]

During a rollover, the warmer liquid from the lower layer transfers to the top, which also causes a sudden pressure drop in the liquid due to the removal of the hydrostatic pressure. This causes a large amount of LNG to evaporate, which is termed as a *flash.* The pressure relief valves do not necessarily have enough capacity to remove the produced BOG, which may in turn cause structural damage to the tank. [45]

The rollover phenomenon can also occur without the addition of a new batch of LNG. In this case, the most important contributing factor is the weathering of the LNG, which causes density differences in the liquid. [42] It should be emphasized that rollover may occur multiple days after refilling of the tank [46], so in normal operation conditions the formation

of stratifications can be observed from density, temperature and BOR measurements. Appropriate actions may then be taken to ensure that no rapid increase occurs in the BOR.

There are a few techniques available to prevent rollover. First and foremost, the formation of stratification can be avoided by taking account the density differences when filling the tank. Typically there exists an option to fill the tank from either the bottom or the top. If a new, lower density cargo is pumped into the tank from the bottom, it will start to transfer to the top driven by the density difference. BOR will increase, but the process is controllable as the pumping process and liquid movement to the top usually takes multiple hours. If the same cargo is pumped to the top, it will remain there and the risk for rollover exists. [47]

Other rollover prevention measures are used to disturb the stratification interface to induce mixing and intentional boil-off. One method includes breaking the layer with nozzles that spray LNG jets inside the tank. Another alternative is to pump LNG from one layer to another, and a third one is to pump LNG out of the tank to vaporizers and utilize it elsewhere. [47] Some LNG operators choose deliberately to fill the tank so that no buoyancy-driven mixing happens [48]. If done correctly, a smaller amount of LNG is lost from the tank due to boil-off. Usually this method is coupled with the third described option (i.e. removing and vaporizing the heel before a rollover occurs). [47]

3.2.4 Rapid phase transition

Rapid phase transition (RPT) is a reaction that may occur between a liquid pool of LNG and warm liquid, such as water. When the two substances are brought into physical contact, an intense heat transfer occurs and a large amount of natural gas vapour is formed. The danger of RPT is twofold: firstly it creates a large amount of cryogenic vapour that could cause further damage or danger to nearby surroundings, and secondly even a relatively small amount causes a large evaporative cloud to form, which in turn can cause sudden pressure spikes and lead to bursting of storage vessels. A further danger is the ignition of the vapour cloud. [43]

RPT is generally a phenomenon that is significant if there are LNG leaks, as under normal operation conditions it should be impossible for LNG to be in contact with water. Naturally,

this means that the LNG that is fed into the tank needs to be dehydrated, and all connections into the tank need to be designed so that no water is capable of getting in. A special occurrence of the phenomena is possible with LNG carriers, as seawater could potentially mix with the tank contents if a breach occurs. [43]

3.3 Previous models

There have been a few areas of interest when it comes to modelling of LNG tanks. One of them is the rollover phenomenon, which has been studied on a handful of papers since the 1970's. Another topic of interest is the sloshing of LNG in marine transport vessels, as well as the rate of evaporation during sea voyages and unloading. A third subject presented in this thesis is the filling of a LNG tank, which has been mainly of interest for the LNG companies and not so much an open literature subject. Other research subjects are generally connected to the supporting facilities, such as liquefaction processes or integration of the cryogenic cycles to supporting the facilities.

3.3.1 Rollover

Previous rollover models can be divided into two categories: lumped parameter (LP) models and distributed numerical models. LP models divide the tank into separate sections, namely into a vapour layer, and two liquid layers separated by an interface. [45] The coupled differential equations that describe the mass and heat balance between the sections are solved, and as a final result it is possible to predict the BOR, ageing properties of the LNG and the time of rollover occurrence. Heat and mass transfer rates can be estimated from empirical correlations, or in the case of inverse methods, directly from the measured data. [48]

Distributed numerical models utilize CFD to model the rollover phenomenon. Current presence of CFD in LNG rollover simulations is quite limited in the open literature. CFD calculations are generally more complex and require long computational times, while requiring also quite specific boundary conditions and initial values. Some issues are also connected to the problematic modelling of the interfaces both in the vapour space and in the stratified layer. [45, 49] Additionally, in the 1970's, when the rollover phenomenon was

discovered and models needed to be developed, CFD calculations were still in infancy. Practically, LNG tank operation is nowadays based on density and temperature measurements coupled with standard procedures and precautions (e.g. tank composition is taken into account during refilling). Thus LP models are more easily integrated into these tank management systems. [45]

The majority of LNG rollover models have been derived from the La Spezia incident from 1971, since it was the best documented case for a long time. First LNG tank rollover models were derived from the stratification models that depicted the behaviour of seawater with different saline concentrations. Later these models were scrapped in favour of the Reynolds-analogy based models. [45] The ROLLO program is one of the few tools available for rollover modelling. ROLLO can be used to calculate the evolution of stratified LNG based on initial temperatures and compositions of the tank. [42] A paper by Arjomandnia et. al. [45] gives a more comprehensive review of the different models used in describing the rollover phenomenon.

As CFD models are not currently implemented in modelling the LNG rollover phenomena, it would be quite challenging to develop a reliable model in the timeframe of this thesis and with the limited amount of data that is easily accessible. Initially, the rollover phenomenon was one of the considered focus points for this thesis, but due to the current state and capabilities of the CFD models the focus shifted more towards the modelling of BOR and describing the flow behaviour inside the tank.

3.3.2 Other models

Koyama [47] investigated the efficient filling of a LNG tank by using CFD. The calculation procedure used an Euler-Euler homogenous multiphase simulation using ANSYS CFX. Heat transfer was modelled along the container walls, as well as the latent heat of evaporation at the liquid surface. However, the mass transfer of evaporation was neglected. The model used a moving boundary to properly simulate the tank liquid level rising in the filling process. The simulation model was verified by measurements. As a result, the study characterised the

most important parameters leading to larger density differences (e.g. initial density difference of the cargo and heel, initial depth of heel, and feed rate).

Other models have been developed, for instance, for determining the pressurizing period of cryogenic tanks [50], BOR estimation [51, 52] and overall BOG handling, system integration and offshore terminals [53, 54, 55]. Another well covered topic is the BOR generation during sea voyages and the sloshing phenomena specific to shipboard membrane tanks [56]. A commercial software called LNG MASTER® has been developed mainly for tank operators. It is capable of modelling LNG unloading, weathering, stratification and rollover phenomena with verified results from a 500 m^3 LNG tank [57].

Carbon dioxide desublimation has mainly been studied in gas mixtures [58, 59, 60, 61], but evidently not with cryogenic liquids. Another quite popular topic has been about heat exchangers capable of desublimating CO_2 [62, 63]. Submerged sublimation that occurs in this thesis is therefore based purely on simplified concepts, as no better references could be found from literature.

3.4 Model theory

In the subsequent sections, the model developed in this thesis is presented. The modelling tool was ANSYS Fluent 15.0. The computational mesh was created using ICEM 15.0, and the post processing was done using MATLAB© and ANSYS Fluent.

There are two main approaches for numerical simulation of multiphase flows: Euler-Euler and Euler-Lagrange. The Euler-Lagrange approach treats the liquid phase as a continuum and the dispersed phase as a large number of particles, bubbles or droplets which are tracked through the calculated flow field. The trajectory of the discrete phase particles is predicted on the basis of the force balance on a given particle. The Euler-Euler approach treats the different phases as interpenetrating continua. A given volume is divided into volume fractions for the different phases, and the continuity and momentum equations are solved for each phase individually. As the Euler-Lagrange approach is more suitable in modelling fluid-particle flows, the model in this thesis is based on the Euler-Euler approach. [64]

ANSYS Fluent has three alternatives for the Euler-Euler multiphase models: mixture model, Eulerian model and volume of fluid (VOF) model. The Eulerian model is the most extensive and complex multiphase model available in ANSYS Fluent. It can be used to model an arbitrary number of phases, and thus offers the greatest versatility in further model development. As such, the Eulerian model approach was chosen for this thesis. Another strong contender for the task is the VOF model, as it is suitable for modelling stratified flows and tank sloshing, while also being computationally less expensive. [64]

3.4.1 General model characteristics

A 2D axisymmetric CFD simulation is performed in this work. The simulation uses an Eulerian multiphase model, which includes the gaseous and liquid phases of pure methane. Carbon dioxide is not modelled as a physical substance, but rather as momentum and energy source terms. The heat and mass transfer between the two methane phases is implemented, along with the typical heat leak rates into the tank walls. Two different definitions for pressure was used: some simulations have a fixed (constant) operational pressure and some simulations use floating operating pressure, which enables the gradual increase of pressure inside the tank. The effect of these two definitions is discussed in more detail in section 4.1.

Model priority has been chosen to be on the modelling of heat and momentum sources in the tank to simulate the injection and desublimation of carbon dioxide. The objective is to see what kind of density differences and flow paths these sources could drive in the system, and how this affects the boil-off rate. This development path was chosen to be the initial objective, and if the model proves to be successful, further model development could be done to properly adjust the model to handle more complex simulations.

As was discussed in section 3.2.3, rollover phenomenon is quite complex and difficult to implement in CFD models, even more so when there is additional CO_2 injection into the tank. Therefore the rollover phenomenon has not been studied in the simulation. However, it should be kept in mind that the rollover phenomenon is fundamentally caused by the formation of stratified layers in the LNG tank, and the CO_2 feeding process might partially contribute to this. In that sense, one needs to be aware of the rollover phenomenon when

evaluating results from the simulations. On the other hand, the CO_2 feeding process is likely to cause large transitions in the tank state in a short time period, which raises a suggestion that it is more critical to evaluate the immediate effects of the feeding process. Furthermore, if an integrated energy storage vessel described in this thesis would be developed, there are already existing technologies (introduced in section 3.2.3) to adapt to the stratification of the LNG and to prevent violent rollover.

The boil-off phenomenon is drastically simplified in this thesis. Typically, the tank houses multiple compounds with different evaporation rates. This thesis assumes that the tank contains only pure methane, so the saturation temperature can simply by expressed as a function of pressure, instead of separate dew and bubble points of multiple different compounds. Boil-off occurs at the surface of the liquid-vapour interface, which is a slightly different approach from the traditional pool boiling occurring between a liquid-solid interface. A simple correlation is used to simulate the boil-off phenomena with mass and heat transfer occurring between the phases.

Modelling is done in two phases: a stable base case and a transient phase. During the stable phase, heat leak from the ambient environment is the only contributing factor to the BOR and flow patterns in the tank, whereas during the transient phase, CO_2 feeding is initiated and desublimation occurs at a given region in the tank. The feed in process is initialized linearly in time, so no sudden shock occurs in the tank. Solver and computational settings are as identical as possible between the different phases of the simulations.

3.4.2 Solver

In ANSYS Fluent, the computational domain is divided into discrete control volumes, for which the conservation equations are solved. In general, the process can be thought to be two-part: integration of the governing equations on the individual control volumes to obtain algebraic equations for the unknown parameters - and a linearization of the discretized equations and solution for updating the parameters. The exact algorithm used to achieve this is dependent on the solver type. [64]

With an Eulerian multiphase model in ANSYS Fluent, the density-based solver is not available, so the pressure-based solver must be used. In the pressure-based solver, velocity field is obtained from momentum equations, and pressure field is obtained by manipulating continuity and momentum equations. Solution may be derived by either using a segregated or a coupled algorithm. Segregated algorithm solves each variable one after another, which makes it memory efficient, but the convergence is slower. Coupled algorithm solves momentum and continuity equations in a coupled manner. Transport equations are solved segregated for additional scalars, such as turbulence. Coupled algorithm requires more memory, but convergence is improved when compared to segregated solver. This work employs a segregated solver, more specifically a phase coupled SIMPLE algorithm for the pressure-velocity coupling. [64]

CFD problems can be either transient or steady state. This work requires the transient solution, as the state in the tank varies with time. The CFD calculation procedure therefore dictates that the governing equations need to be discretized in both space and time. To clarify, the general transport equation for a scalar quantity ϕ may be written as

$$\int_V \frac{\partial \rho \phi}{\partial t} dV + \oint \rho \phi \boldsymbol{v} \cdot d\boldsymbol{A} = \oint \Gamma_\phi \nabla_\phi \cdot d\boldsymbol{A} + \int_V S_\phi dV \tag{1}$$

where ρ is the density, V is the volume, $\boldsymbol{v}$ is the velocity vector, $\boldsymbol{A}$ is the surface vector, Γ_ϕ is the diffusion coefficient for ϕ, ∇_ϕ is the gradient of ϕ and S_ϕ is the source term per unit volume. In equation (1), the first term corresponds to change of property ϕ with time, the second term is the convective term, the third term is the diffusion term and the final term is the source term. Spatial discretization of the previous equation yields

$$\frac{\partial \rho \phi}{\partial t} V + \sum_f^{N_{\text{faces}}} \rho_f \boldsymbol{v}_f \phi_f \cdot \boldsymbol{A}_f = \sum_f^{N_{\text{faces}}} \Gamma_f \nabla_f \phi_f \cdot \boldsymbol{A}_f + S_\phi V \tag{2}$$

where N_{faces} is the number of faces enclosing the computational cell and f corresponds to a given face. The face values are used in the actual calculations, and the derivation of these face values can be done by using some discretization method. In this thesis the upwind scheme is used, which derives the face values from the cell upstream values relative to the direction of the normal velocity. [64]

Temporal discretization can be done by using either an explicit or implicit method. Implicit methods may further be divided into time-dependent and steady-state schemes, while the explicit method is purely for time-dependent problems. In this thesis an implicit formulation with a time-dependent scheme is used, which makes the algorithm time-marching. The implicit method calculates the evolution of a variable based on both the previous and current time step through an iterative process. Generally speaking, the benefit of the implicit method is that it is more stable with respect to time step size when compared to the explicit method, which uses only values from the previous time step in the calculations. [64]

The geometric reconstruction scheme uses standard interpolation schemes for the face fluxes in the cells which are completely filled with one phase. In boundary cells, which contain both phases, the geometric reconstruction scheme is used. A piecewise-linear boundary is constructed between the phases, and the advection of the fluid is calculated through the cell faces according to this boundary. The geometric reconstruction scheme produces a sharp interface, and is as such well suited for modelling a liquid-vapour interface in a tank. [64]

The selection of the turbulence model is a one further decision that a CFD calculation procedure requires. This work uses the k-ε standard model, which is a widely used two-equation turbulence model. Turbulence is characterised in this model by two transport equations, one for the turbulent kinetic energy k and another for the dissipation rate ε. The k-ε-model is a robust, economic turbulence model employed in a wide range of applications [64]. For this study, the k-ε-model was chosen mainly for its relatively low computational expense and good overall stability.

3.4.3 Conservation equations

The conservation of mass is given by the continuity equation which can be written for a phase q in discretized form

$$\frac{\partial}{\partial t}\left(x_{\mathrm{q}}\rho_{\mathrm{q}}\right) + \nabla \cdot \left(x_{\mathrm{q}}\rho_{\mathrm{q}}\boldsymbol{v}_{\mathrm{q}}\right) = \sum_{p=1}^{n}\left(\dot{m}_{\mathrm{pq}} - \dot{m}_{\mathrm{qp}}\right) + S_{\mathrm{q}} \tag{3}$$

where t is time and x is the volume fraction. The subscripts p and q refer to different phases, and n describes the number of phases. Finally, the term $\dot{m}_{\mathrm{pq}}$ describes mass transfer from phase p to q [64]. In this work, the additional source term S is not used in the continuity equation, but rather the mass transfer between the methane phases is implemented through a user-defined function.

The conservation of momentum is described by the equation

$$\begin{aligned}\frac{\partial}{\partial t}\left(x_{\mathrm{q}}\rho_{\mathrm{q}}\boldsymbol{v}_{\mathrm{q}}\right) + \nabla\cdot\left(\mathrm{x}_{\mathrm{q}}\rho_{\mathrm{q}}\boldsymbol{v}_{\mathrm{q}}\boldsymbol{v}_{\mathrm{q}}\right) \\ = -x_{\mathrm{q}}\nabla p + \nabla\cdot\bar{\bar{\tau}}_{q} + x_{\mathrm{q}}\rho_{\mathrm{q}}\boldsymbol{g} \\ + \sum_{p=1}^{n}\left(\boldsymbol{R}_{\mathrm{pq}} + \dot{m}_{\mathrm{pq}}\boldsymbol{v}_{\mathrm{pq}} - \dot{m}_{\mathrm{qp}}\boldsymbol{v}_{\mathrm{qp}}\right) + \left(\boldsymbol{F}_{\mathrm{q}} + \boldsymbol{F}_{lift,\mathrm{q}} + \boldsymbol{F}_{\mathrm{vm,q}}\right)\end{aligned} \tag{4}$$

where p is the static pressure, $\bar{\bar{\tau}}$ is the q^{th} phase stress-strain tensor, $\boldsymbol{g}$ is the gravitational acceleration and R is the interaction force between phases. The last three force terms are the external body force, the lift force and the virtual mass force, respectively. [64]

ANSYS Fluent assumes that each secondary phase forms bubbles or droplets. The interaction force R is defined as

$$R = \frac{x_{\mathrm{q}}x_{\mathrm{p}}\rho_{\mathrm{p}}f}{\tau_{\mathrm{p}}}\left(\boldsymbol{v}_{\mathrm{p}} - \boldsymbol{v}_{\mathrm{q}}\right) \tag{5}$$

where f is the drag function and τ is the particulate relaxation time, which is defined as a function of density, viscosity, friction factor and the droplet diameter. [64] A default droplet diameter of 0.01 mm was assumed for the vapour phase as no better estimate could be found.

The drag function f from equation (5) is defined distinctly for different types of problems. In this thesis, the symmetric drag function is used, as it functions well when the secondary phase becomes the dominant phase in another region of the domain. The symmetric model calculates the density and viscosity from the volume averaged properties and defines the drag function as a function of the Reynolds number. [64, 65]

The conservation of energy is written as

$$\frac{\partial}{\partial t}\left(x_{\mathrm{q}}\rho_{\mathrm{q}}h_{\mathrm{q}}\right)+\nabla\cdot\left(\mathrm{x}_{\mathrm{q}}\rho_{\mathrm{q}}\boldsymbol{v}_{\mathrm{q}}h_{\mathrm{q}}\right)$$
$$=x_{\mathrm{q}}\frac{\partial p_{\mathrm{q}}}{\partial t}+\bar{\bar{\tau}}_{q}:\nabla\boldsymbol{v}_{\mathrm{q}}-\nabla\cdot\boldsymbol{q}_{\mathrm{q}}+S_{\mathrm{q}} \tag{6}$$
$$+\sum_{p=1}^{n}\left(Q_{\mathrm{pq}}+\dot{m}_{\mathrm{pq}}h_{\mathrm{pq}}-\dot{m}_{\mathrm{qp}}h_{\mathrm{qp}}\right)$$

where h is the specific enthalpy, $\boldsymbol{q}$ is the heat flux and Q is the intensity of heat exchange between the phases. [64] For clarification, the h_{pq} term refers to the latent heat change between phases p and q, whereas the h_{q} term corresponds to the specific enthalpy of a given substance.

3.4.4 Evaporation-condensation model

Fluent natively supports the option to include the evaporation-condensation model in Eulerian multiphase simulations, but in this thesis it was nevertheless implemented through a user-defined function (UDF) in order to gain a greater flexibility. Vapour mass transfer (continuity) equation was introduced in the previous section. In general form without the source term, the equation can be written as

$$\frac{\partial}{\partial t}\left(x\rho_{\mathrm{p}}\right)+\nabla\cdot\left(x\rho_{\mathrm{p}}\boldsymbol{v}_{\mathrm{p}}\right)=\dot{m}_{\mathrm{qp}}-\dot{m}_{\mathrm{pq}} \tag{7}$$

The mass transfer from liquid to vapour phase is assumed if the liquid temperature in the computational cell is larger than the saturation temperature ($T_{\mathrm{l}}>T_{\mathrm{sat}}$). Thus the mass transfer can be written from phase *q* to phase *p*

$$\dot{m}_{qp}=cx_{\mathrm{q}}\rho_{\mathrm{q}}\frac{T_{\mathrm{q}}-T_{\mathrm{sat}}}{T_{\mathrm{sat}}} \tag{8}$$

and conversely from phase *p* to phase *q* ($T_{\mathrm{v}}<T_{\mathrm{sat}}$)

$$\dot{m}_{pq}=cx_{\mathrm{p}}\rho_{\mathrm{p}}\frac{T_{\mathrm{p}}-T_{\mathrm{sat}}}{T_{\mathrm{sat}}} \tag{9}$$

where T_{sat} is the saturation temperature, which has been defined as a function of pressure (equation 12). The coefficient c is a time relaxation factor, which was fixed through an up-and-down method to the value of 0.02. With the chosen coefficient, the BOR which was obtained from Fluent agreed with the BOR calculated from the energy balance. The

coefficient seeking was done during the preliminary simulation (i.e. no CO_2 feeding, so the only driving force for BOR was the heat leaks into the tank). The source term for the energy equation is simply obtained by multiplying the given mass transfer by the specific latent heat of evaporation, as was presented in equation (6). [64]

In addition, the Ranz-Marshall heat exchange model was set between the vapour and liquid phase. The validity of Ranz-Marshall model for this simulation has not been evaluated, and for future simulations a more appropriate model could be chosen. The heat exchange model affects especially to the liquid-vapour interface temperature distribution.

3.4.5 Desublimation of carbon dioxide

In this thesis, it is assumed that the carbon dioxide is brought to the bottom of the tank in gaseous phase. In the vicinity of the inlet, the carbon dioxide will solidify through desublimation as the vapour is brought into contact with the cryogenic LNG. As the density of the solid CO_2 is considerably larger than the density of the liquid phase, it is assumed that the solid particles settle on the bottom of the tank. In the simulation model, the solid accumulation has not been implemented. As the density ratio between the vapour and solid phase is measured in the hundreds, the desublimation process could potentially cause sudden variations in the local conditions (e.g. pressure) as the volume decreases radically. Physical volume occupied by the solid phase is likely to be quite negligible. If the conditions are suitable, it could also be possible that the solid particles could be carried away by the flow and dispersed in the tank. So far the exact mechanisms and reactions that could occur during the desublimation are unclear and would likely require physical experiments.

No studies were found which would assess the effects of desublimating CO_2 while being injected to a cryogenic liquid. Same applies also to the desublimation of pure CO_2 by utilizing a cryogenic gas, such as the BOG in LNG tanks. There is, however, an experimental study which investigated the rate of desublimation of a nitrogen-CO_2-gas mixture (with CO_2 content of 5-16 % of volume) on a cooled plate [58]. A further mathematical model for shell-and-tube type heat exchangers was also developed [62]. The studies concluded that it could be possible to capture CO_2 from a gas mixture resembling purified flue gases, and that the technology would require periodic removal of the frozen particles from the heat exchanger's

surfaces to maintain decent efficiency. The presented studies gave little insight on the behaviour of desublimated CO_2, and thus the model implemented in this thesis is quite crude and elementary (i.e. only heat and momentum source terms are used, and the actual phenomenon is not modelled).

There are multiple alternative structural solutions for injecting the carbon dioxide inside the tank, and the bottom-feed solution presented in this thesis is just one alternative. It is likely that a realistic solution would require multiple alternative inlet options so that the feeding process could adapt to the conditions in the tank, similarly to the current LNG refilling process. In any case, it is important to understand the basic flow behaviour if the feeding is implemented from the bottom section of the tank.

One of the possible injector alternatives could be a nozzle or a group of nozzles, which could potentially utilize the Joule-Thomson phenomenon to rapidly cool down the CO_2 without causing excess heating of the cryogenic LNG due to minimization of the sensible heat brought into the tank. Actual feasibility of such an assembly is quite hard to evaluate without comprehensive understanding of the phenomenon and extensive testing.

Another important aspect to note is the flow patterns that would arise from the injection. One large inlet pointed towards the bottom of the tank is likely to cause large turbulence and potent flow mixing in the tank. Smaller inlets spread throughout the tank at given locations would be technically harder to achieve, but could potentially offer benefits in the resulting flow behaviour. Clogging of the inlet pipes is one major concern that should be assessed through physical experiments. In the worst-case scenario, desublimation region could reach the interior, freeze the pipe and prevent flow into the tank.

Clearly it is a large challenge to remove the stored carbon dioxide out from the tank once it has been stored among the liquid. Thermal removal (by introducing heat into the stored lump of carbon dioxide) would essentially also mean that some of the cryogenic liquid is evaporated simultaneously, which may not be beneficial since the tank is supposed to be operating in energy storage mode at that time. Furthermore, a gas separation process would be required to separate the evaporated hydrocarbons from the regasified carbon dioxide.

Thus physical removal from the tank should also be considered as one alternative. Using this approach the thermal energy released by sublimation could potentially be used in other parts of the process. However, the technical limitations may prove to be challenging, as for instance no pipe penetrations in the wetted area of the tank should be done, and maintenance of the mechanical components can be challenging.

In this thesis, desublimation is modelled by implementing an energy and momentum source term via a UDF into a given volume of the tank. An arbitrary cylindrical volume near the CO_2 inlet was defined to be the only region where desublimation occurs. The amount of CO_2 fed into the tank has been estimated by integrating the storage tank to an oxy-fuel combustion plant. A more detailed procedure for evaluating the numerical values for the energy and momentum source terms has been introduced in section 3.6.

3.5 Material properties

Section 2.3. demonstrated that natural gas is mainly composed of methane, so the model in this thesis will be based on the material properties of pure methane. In further studies, a more realistic composition for LNG could be derived by incorporating heavier hydrocarbon components and nitrogen into the model, and defining the material properties based on the mixture rules. The material properties of carbon dioxide are also introduced in this section, as they are crucial in determining some boundary values for the simulations.

3.5.1 Phase diagrams

Figure 16 shows the phase diagram of methane at the operational range. At a pressure of roughly 1 bar, the saturation temperature of methane is slightly below 112 K. In this paper, the bulk temperature of methane has been chosen so that it corresponds to the saturation temperature at the operational pressure, which also typically holds true for LNG storage tanks.

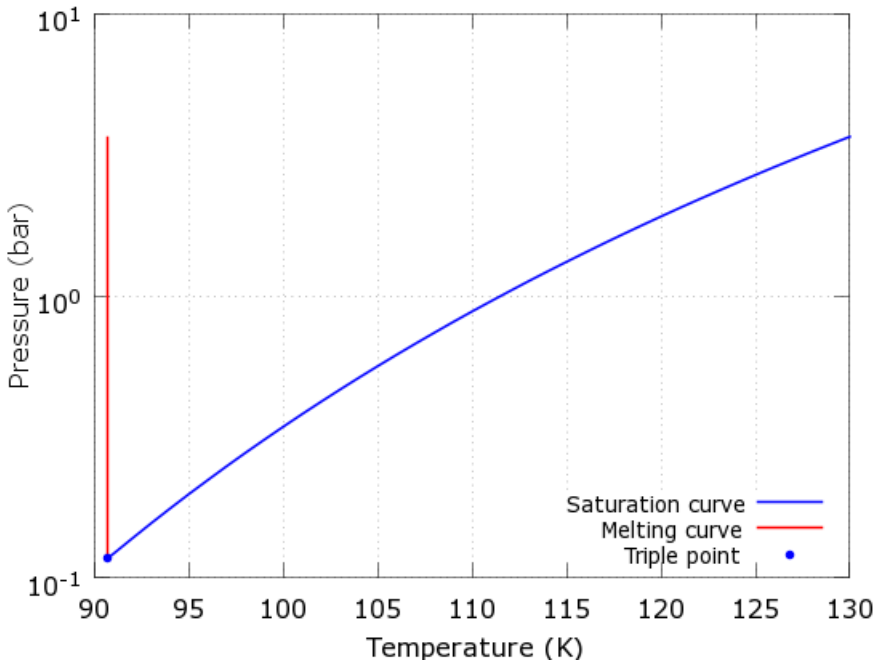

Figure 16: Phase diagram of methane in the cryogenic temperature range.

The phase diagram of carbon dioxide is shown in figure 17. The triple point of carbon dioxide is at 216 K and 5.17 bar. Below this pressure, carbon dioxide cannot be liquefied. Conversely, if the pressure in the inlet pipe should exceed 5.17 bar, the carbon dioxide could liquefy. This phenomenon should be taken into account in more detailed design of the system, as the liquefaction could potentially cause problems in the pumping or piping systems due to the existence of two phases in the fluid.

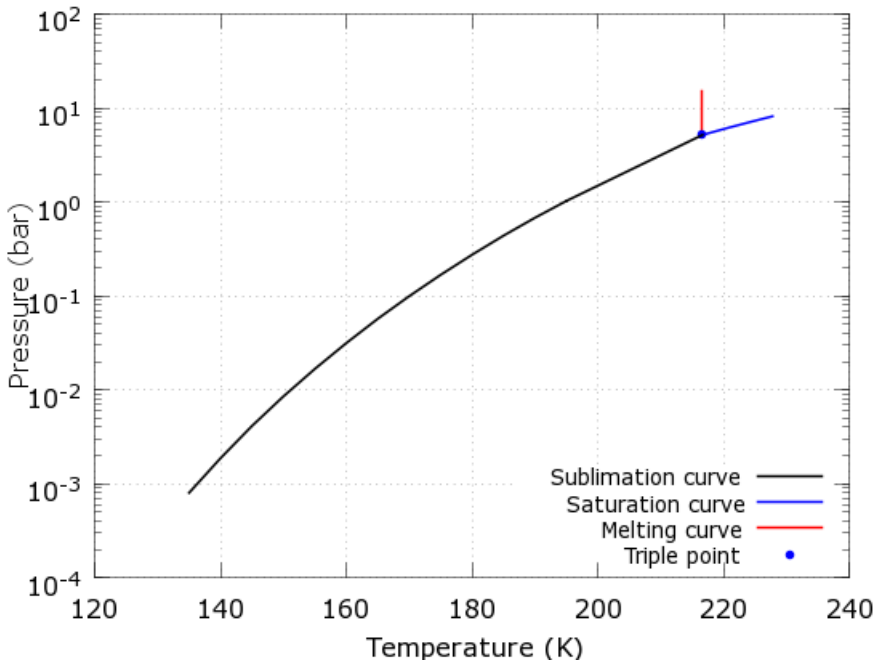

Figure 17. Phase diagram of carbon dioxide near the operational temperature range.

Density of liquid methane at a temperature of 112 K and pressure of 1 bar is roughly 425 kg/m^3. For this study, the height of the LNG tank was chosen to be 40m. Thus, the hydrostatic pressure p_h at the bottom of the tank can be calculated by

$$p_\mathrm{h} = \rho g h \tag{10}$$

where h is the height of the tank. By using a fixed value for the density, the hydrostatic head can be calculated to be at most

$$p_\mathrm{h} = 425\frac{\mathrm{kg}}{\mathrm{m}^3} \cdot 9.81\frac{\mathrm{m}}{\mathrm{s}^2} \cdot 40\ \mathrm{m} \approx 167\ \mathrm{kPa}$$

Thus the sum of hydrostatic and ambient pressure at the bottom of a 40 m high LNG layer is about 2.7 bar, so technically it should be feasible to feed CO_2 into the tank even from the bottom section and still remain at a pressure level which is below the triple point. One further aspect that should be considered is the state of the inlet pipe when the feeding process is not ongoing: if the pressure at the other end of the inlet pipe is too low, some of the liquid inside the tank will creep up the inlet pipe, potentially causing clogging when carbon dioxide feeding process is initiated again.

What can also be seen from figure 17 is that the sublimation of the solid CO_2 back to gas (or liquid) form might be difficult: if the solid carbon dioxide is stored in the same compartment

with the liquefied methane, it will cool in solid form to the same storage temperature as methane, and the removal of CO_2 from the storage would require an equal amount of heat to be brought into the carbon dioxide to cause the reverse phase change. Naturally, some of this heat is inevitably absorbed by methane, which could cause unwanted BOG losses.

In this thesis, it is assumed that the carbon dioxide is injected into the tank at a temperature of 190 K. This value was chosen mainly due to the availability of thermodynamic phase change data. In reality, the inlet temperature of the carbon dioxide is limited by the *operational pressure* in the tank. Simply put, the lower the pressure of the CO_2 is in inlet conditions, the colder it may be. Thus, if the tank is operating in approximately ambient pressure, the inlet temperature of CO_2 must be higher than the previously mentioned 190 K – otherwise the inlet pressure of the CO_2 would be lower than in the tank and the flow would be reversed. In that sense, the chosen inlet temperature can be considered to be a best-case scenario, as it results in the lowest amount of sensible heat brought into the tank. If the CO_2 is fed to the bottom of the tank the effect of hydrostatic pressure must also be considered. In other words, when CO_2 is fed into the bottom of the tank, the inlet temperature could theoretically be slightly higher than that of near-surface feeding.

The inlet temperature of the carbon dioxide mainly affects to the amount of energy brought into the tank. Specifically three different heat exchange stages can be identified in the feed-in process: cooling of the gaseous CO_2, desublimation, and finally cooling in the solid state. The cooling of the gaseous CO_2 has been left outside this study, as no thermodynamic data was found for the vapour phase covering the desired temperatures. Additionally, the temperature difference is likely to be quite small, as it is beneficial to capture the thermal energy of CO_2 for other processes of the integrated storage concept. In-detail analysis would also require an accurate estimation of the inlet pressure – which in turn requires full modelling of the cycle.

In conclusion, the assumptions made in this thesis are that the sublimation occurs somewhere in the temperature range of 190-216 K, and that the solid CO_2 cools down from 190 K to 110 K. The effect of cooling the gaseous CO_2 is considered insignificant in this thesis. As

stated before, these assumptions and temperature ranges are somewhat restricted by the availability of the thermodynamic data and the lack of in-detail cycle analysis.

3.5.2 Thermodynamic properties

In this thesis, most of the material properties have been defined as constant values, which have been collected to table 2. All the constant material properties were evaluated at a pressure of 103.8 kPa and the temperature corresponding to the saturation temperature of methane at that pressure. Density of the vapour phase has been modelled using the Soave-Redlich-Kwong (SRK) real gas model. The density of the liquid phase has been set as a constant value. The use of this simplification is justified as the liquid phase experiences only a slight variation in density from pressure changes. The Boussinesq approximation is used to model the buoyant movement of the liquid. The Boussinesq model employs constant density for the liquid, but introduces a temperature-driven buoyancy term in the momentum equation.

Table 2. Material properties of methane for CFD simulation. [28, 24]

	Liquid	Vapour	
Density	422	SRK	kg/m^3
Molecular weight	16.04		kg/kmol
Specific heat capacity	3469.1	1820	J/kgK
Thermal conductivity	0.1862	0.0118	W/mK
Dynamic viscosity	121.36	4.48	μPa-s
Standard state enthalpy	-74.85		kJ/kmol
Standard state entropy	186160		J/kgmolK
Critical temperature	190.564		K
Critical pressure	4599.2		kPa
Critical specific volume	6.147793		m^3/g
Acentric factor	0.01142		
Latent heat of evaporation	536		kJ/kg
Initial bulk temperature	112		K
Thermal expansion coefficient	0.033		1/K

Reference state for the standard state enthalpy and entropy is 298 K and 1 atm. The properties for carbon dioxide are shown in table 3. The value for the specific heat capacity of solid carbon dioxide was estimated as a constant value on the temperature range 110 – 190 K.

Table 3. Material properties of carbon dioxide. [66, 67, 28]

Specific heat capacity	1.14	kJ/kg-K
Difference between feed-in and storage temperature	80	K
Latent heat of sublimation	593	kJ/kg
Density of gas at feed outlet, at 2.8 bar, 216 K (used only for the calculation of flow velocity inside the inlet pipe)	7.14	kg/m^3

One more correlation is required for the evaporation-condensation model to access the saturation temperature of methane. The correlation requires pressure p in bar as an input value, and the returned value is saturation temperature in Kelvin. Validity range is 0.9 – 3.16 bar, which corresponds to saturation temperatures of 110.5 – 127.3 K. The correlation is implemented in ANSYS Fluent as a UDF. The correlation is

$$T_{\mathrm{sat}}(p) = -1.53647p^2 + 13.6216p + 99.5619 \quad (11)$$

3.6 Dimensions and boundary conditions

The dimensions of a typical onshore flat bottom LNG tank are used to evaluate the height and diameter of the tank. Similarly, the heat leak rates into the container were evaluated from typical values of existing LNG tanks [51, 45, 46, 68, 38].

Maximum design gauge pressure in the tank is 50 kPa [69], and typically the operating gauge is pressure is in range 5 - 35 kPa [30, 42, 51, 29]. The maximum gauge pressure is typically restricted by the mechanical structure of the tank, and a slight overpressure is required to guarantee that ambient air is unable to get in - otherwise the condensing nitrogen and moisture could cause various problems inside the tank (e.g. RPT, corrosion, stratification). In this work the chosen gauge pressure was 2.5 kPa, which is below the usual limits. Correction of the pressure would have required a complete overhaul of the simulations, so a slight variation from typical values was in this case accepted.

Inlet pipe diameter was chosen to be 0.9 m, which is enough to maintain flow velocity of the CO_2 at a reasonable level (roughly 2.8 m/s with 100 % load). The values required to calculate this flow velocity are introduced in the next chapters, but the process is not explained in detail. With a 15 cm thick wall and insulation the total outer diameter of the pipe is 1.2 m, which is quite close to the diameter of the LNG inlet pipes in existing tanks [32]. It is possible that the CO_2 feeding procedure requires multiple inlets with slightly smaller diameters, but for the sake of simplicity this simulation operates with only one inlet pipe.

One of the largest uncertainties lies in the estimation of the desublimation area. No better estimation could be found in literature, so the desublimation region was simply chosen to extend 1 m downward from the inlet pipe exit. The pipe outlet was also chosen to be located at a height of 3 m from the tank floor. Table 4 includes the most critical dimensions and properties of the tank and other parameters used in the simulations.

Table 4. Dimensions and properties of the tank.

Tank height	40	m
Tank diameter	50	m
Tank volume	78540	m^3
Liquid level	34	m
Ambient pressure	101325	Pa
Gauge pressure	2500	Pa
BOR	0.08	$\%_{vol}$/day
Heat flux, floor	38	W/m^2
Heat flux, side walls (wet)	10	W/m^2
Heat flux, side walls (dry)	6	W/m^2
Heat flux, roof	13	W/m^2
CO_2 inlet pipe radius	0.45	m
CO_2 inlet pipe wall thickness	0.15	m
CO_2 inlet area length	1	m
CO2 pipe distance from bottom	2	m

In an axisymmetric simulation, one two-dimensional slice of the physical volume can be modelled, and by rotating the given slice 360° around a given axis gives the three-dimensional volume, is a cylindrical tank in this case. Figure 18 shows a two-dimensional presentation of the computational domain. The rotational axis is now on the right hand side, where one can also see the CO_2 inlet pipe reaching three meters above the tank floor. Below the pipe is the desublimation region, which has been confined to a cylindrical shape with the same inner diameter as the pipe and the length of 1 meter.

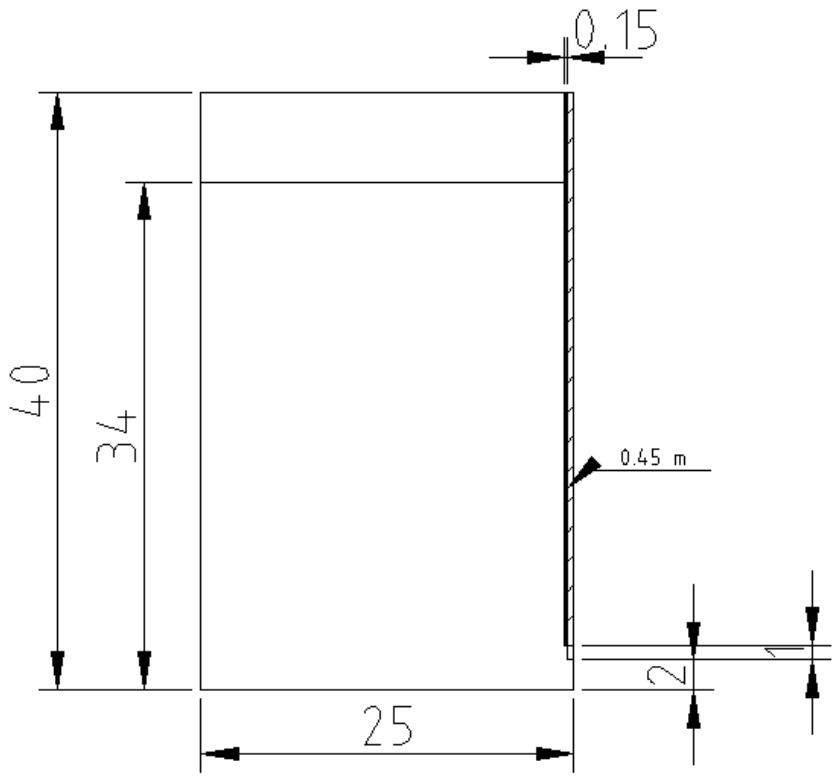

Figure 18. Tank dimensions in meters. CO_2 inlet pipe and feeding region visible at the right hand side. Liquid level was initialized to 34 meters.

Traditionally, the aim in conventional LNG tanks has been to minimize all possible heat leaks into the tank, which also lowers the self-discharge rate of LNG. The BOG generated by the heat leaks is captured from the tank, and additional LNG can be pumped to vaporizers and used in different applications. The integrated energy storage system considered in this thesis is intended to be connected to an oxy-fuel combustion cycle with a gas turbine. One possible benefit of using such a system lies in the more efficient utilization of the latent heat of the substances. For instance, the desublimation energy of carbon dioxide could be utilized to deliberately increase BOR, which is actually desirable when the intent is to use the BOG in a combustion process to produce electricity during peak load demands.

3.6.1 Power plant

The nominal power of this oxy-fuel combustion plant can be estimated on the basis of full load hours and the energy content of the storage tank. With an assumption of 2000 full load hours the plant would have a thermal power of roughly 230 MW. The 2000 full load hours

can be recognized as a reasonable assumption for a plant operating as a seasonal energy storage. Oxy-fuel combustion of methane is described by the chemical reaction

$$\mathrm{CH_4 + 2O_2 \rightarrow CO_2 + 2H_2O} \tag{12}$$

which states that the molar amount of carbon dioxide produced in the reaction is equal to the molar amount of methane combusted. Therefore, the mass ratio of carbon dioxide to methane is given by

$$n_{\mathrm{CO_2}} = n_{\mathrm{CH_4}} \Leftrightarrow \frac{m_{\mathrm{CO_2}}}{m_{\mathrm{CH_4}}} = \frac{M_{\mathrm{CO_2}}}{M_{\mathrm{CH_4}}} \tag{13}$$

where M is the molar mass of each substance. Thus, for each kilogram of methane combusted, 2.7 kilograms of carbon dioxide is formed. The mass flow rate of methane can be calculated from the thermal power P_{th} of the plant

$$\dot{m} = \frac{P_{\mathrm{th}}}{q_{\mathrm{i}}} \tag{14}$$

where q_{i} is the lower heating value. The mass flow rate for methane is

$$\dot{m}_{CH_4} = \frac{230\ \mathrm{MW}}{49.32\ \frac{\mathrm{MJ}}{\mathrm{kg}}} \approx 4.6\ \frac{\mathrm{kg}}{s}$$

and for the carbon dioxide the mass flow rate is 2.7 times larger, 12.7 kg/s.

3.6.2 Boil-off rate and cycle integration

The conceptual idea investigated in this thesis is the feeding of the carbon dioxide from the flue gases into the integrated cryogenic storage tank. The carbon dioxide formed in the combustion process must be precooled, after which it is fed to the tank where it will desublimate and cool in solid form to the bulk temperature of the liquid. As was discussed earlier, the sensible heat required to precool the carbon dioxide in gaseous form has been omitted. The heat brought to the liquid by the carbon dioxide is therefore obtained by summing the latent heat of sublimation (h_{lat}) and the sensible heat of cooling in solid form (h_{sen}). Amount of heat extracted per kilogram (h) of carbon dioxide is

$$h = h_{\mathrm{lat}} + h_{\mathrm{sen}} = h_{\mathrm{lat}} + c_{\mathrm{p}}\Delta T \tag{15}$$

where c_{p} is the specific heat capacity and ΔT the temperature difference between the feed-in and the final temperature. Substituting the numerical values yields

$$593\,\frac{\mathrm{kJ}}{\mathrm{kg}} + 1.24\,\frac{\mathrm{kJ}}{\mathrm{kg \cdot K}} \cdot (190 - 110)\mathrm{K} \approx 690\ \frac{\mathrm{kJ}}{\mathrm{kg}}$$

Thermal power brought into the tank with the carbon dioxide is then

$$P_{\text{th}} = h \cdot \dot{m}_{\text{CO}_2} \tag{16}$$

By substituting the numerical values, the thermal power can be calculated to be

$$P_{\text{th}} = 690\frac{\text{kJ}}{\text{kg}} \cdot 12.7\frac{\text{kg}}{\text{s}} \approx 8.8\ \text{MW}$$

Substituting the calculated thermal power into equation (14), and replacing the lower heating value with the latent heat of evaporation for methane gives the boil-off rate $\dot{m}_{\text{BOG}}$

$$\dot{m}_{\text{BOG}} = \frac{8.8\ \text{MW}}{536\ \frac{\text{kJ}}{\text{kg}}} \approx 16.4\ \frac{\text{kg}}{s}$$

which corresponds to the thermal power of roughly 800 MW when combusted. Evidently, this introduces a problem as the previously chosen capacity for the combustion plant was merely 230 MW. Thus, only a portion of the carbon dioxide could be fed into the tank, or an alternative use must be developed for the additional BOG. In a shorter timescale, the dynamic behaviour and mixing of the tank is in a critical role when assessing the delay and magnitude of the BOR increase.

However, so far we have not calculated the amount of latent heat that could be absorbed by the evaporation of methane. With a constant rate of 4.6 kg/s of methane being removed from the tank in liquid form, the power required to evaporate such amount can be calculated by equation (16) by substituting the material properties for methane (only the latent heat is considered):

$$P_{\text{th}} = 536\frac{\text{kJ}}{\text{kg}} \cdot 4.6\ \frac{\text{kg}}{\text{s}} \approx 2.5\ \text{MW}$$

The oxy-fuel combustion cycle also includes oxygen as a reactant. If the oxygen is stored in liquid form, the latent heat required to evaporate the required amount of oxygen may be derived similarly. Thus the thermal power can be calculated to be roughly 3.9 MW. Together, the phase changes of methane and oxygen amount to 6.5 MW, which is still 2 MW short of the power required to desublimate 12.7 kg/s of carbon dioxide. Figure 19 presents a simplified diagram of the CO_2 mass flow. It can be seen from the figure that potentially 45 % of the CO2 mass flow could be desublimated by oxygen, and respectively 28 – 55 % by the methane stored in the tank. The 55 % value would mean that excess BOG would have to be dumped to an external location, such as a natural gas network. These values were taken into account when choosing the simulation conditions, as is shown in section 3.8.

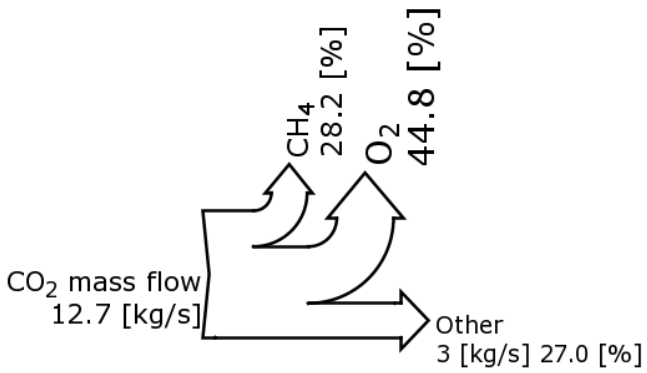

Figure 19. CO_2 mass flow diagram. Methane could be used to desublimate 28 % of the CO_2, and oxygen respectively 45 %. The remaining 27 % of CO2 still needs a source of cold to achieve phase change.

In summary, the overall energy balance states that by evaporating 4.6 kg/s of methane, desublimating 12.7 kg/s of carbon dioxide and evaporating 18.5 kg/s of oxygen, the excess thermal power brought into the tank is roughly 2 MW, which corresponds to an excess boil-off gas generation of 4 kg/s or 200 MW_{th}. However, as the boil-off gas is in an easily utilizable form, it would be quite straightforward to feed the excess boil-off gas to a natural gas grid, for example. This could potentially help in creating a buffer which would complement the larger need for district heating during the winter in colder regions, as the energy storage plant is likely to be running in energy discharge mode during the winter time. The drawback of this technique is that some carbon dioxide is released outside the loop, and the process is not completely closed if the carbon cycle is concerned.

It should also be noted that in the previous assessment it was assumed that all of the heat released and absorbed between the phase reactions could be used with 100 % efficiency in other parts of the process. In reality, it is challenging to build a heat exchange method that is capable of accomplishing this, let alone when the process needs to be reversible (e.g. desublimating carbon dioxide while the oxy-fuel combustion is in operation - sublimating when the electrolysis is in operation). Also, as was previously mentioned, it was assumed that the carbon dioxide has been precooled to 190 K prior to being fed into the tank, and this process requires a source of cold which could be derivable from the process integration. The sensible heat of oxygen, among many other potential exergy sources, has been left outside this evaluation. For complete understanding of the cycle, a more accurate model including

all of the available heat, storage temperatures and realistic operation pressures should be developed. The actual feasibility of such a looping process has been left outside the scope of this thesis.

A similar concept integrating LNG cold exergy utilization with power generation cycle has been proposed by Zhang and Liorm, for example [70]. Zhang and Lior performed thermodynamic modelling of a process combining the Rankine and Brayton cycles with the heat utilization from LNG evaporation. Carbon dioxide, which functions as the working fluid in the process, is precooled by the LNG which simultaneously evaporates. A small fraction (~4%) of the natural gas is sent to the combustion chamber, while the remaining amount is fed to the natural gas grid. Tagliafico et. al. [71] provides an overview on the different energy saving capabilities of different configurations by utilizing the LNG evaporation integration. The largest exergy gains are available in sites utilizing *submerged combustion vaporization*, which uses a fraction of the LNG in a combustion process for the evaporation. *Open rack vaporization*, which is another common evaporation technique, employs sea water with a heat exchanger to evaporate the LNG. [71]

3.6.3 Desublimation

The desublimation of CO_2 was modelled by using energy and momentum source terms in the corresponding equations. An arbitrary volume near the inlet was defined to be the only region where desublimation occurs, and the source terms were introduced to that region. The simulation cases are differentiated from each other by using two parameters which have been named in this thesis as CO_2 *feed condition* and *momentum condition*.

The CO_2 *feed condition* is given as a percentage of the thermal power calculated by equation (16) (i.e. the thermal power required to desublimate CO_2 from flue gases that are formed in combustion process with nominal power). Thus it can be considered to be the portion of the flue gases that are fed into the tank, so in other words a 50 % CO_2 feed condition would mean that exactly half of the flue gases are fed into the tank (and precooled to 190 K before that). With this formulation, the source term for ANSYS Fluent can be derived by dividing the resulting thermal power with the known volume of the desublimation region. The actual numerical values are introduced in section 3.8.

The *momentum condition* is simply the absolute value of the momentum source term plugged into ANSYS Fluent. The final chosen values require some background information before being introduced. Some preliminary test runs were done, which indicated that two distinct flow patterns could potentially arise: one caused by natural convection and another dominated by the momentum source term, which results in a forced flow.

The nature of a flow containing both natural and forced convection can be described by the ratio between Grashof number (Gr) and the square of Reynolds number (Re)

$$\frac{\mathrm{Gr}}{\mathrm{Re}^2} = \frac{g\beta\Delta T L}{w^2} \tag{17}$$

where L is the characteristic length, w is the flow velocity, ΔT is the temperature difference and β is the thermal expansion coefficient. If the ratio is greater than one, the flow is dominated by the natural convection, and conversely values below one correspond to the situations where forced flow is dominant. [72]

For estimative purposes, fixed values can be set for everything else in equation (17) except for the velocity and temperature difference. Characteristic length is taken as the approximate length from the bottom of the tank to the liquid surface. The ratio of the two dimensionless numbers can thus be depicted in a three dimensional coordinate system featuring velocity and temperature as the x-y-plane, as has been done in figure 20. The $\mathrm{Gr}/\mathrm{Re}^2$ ratio of 1 has been highlighted by a plane (which has been coloured red).

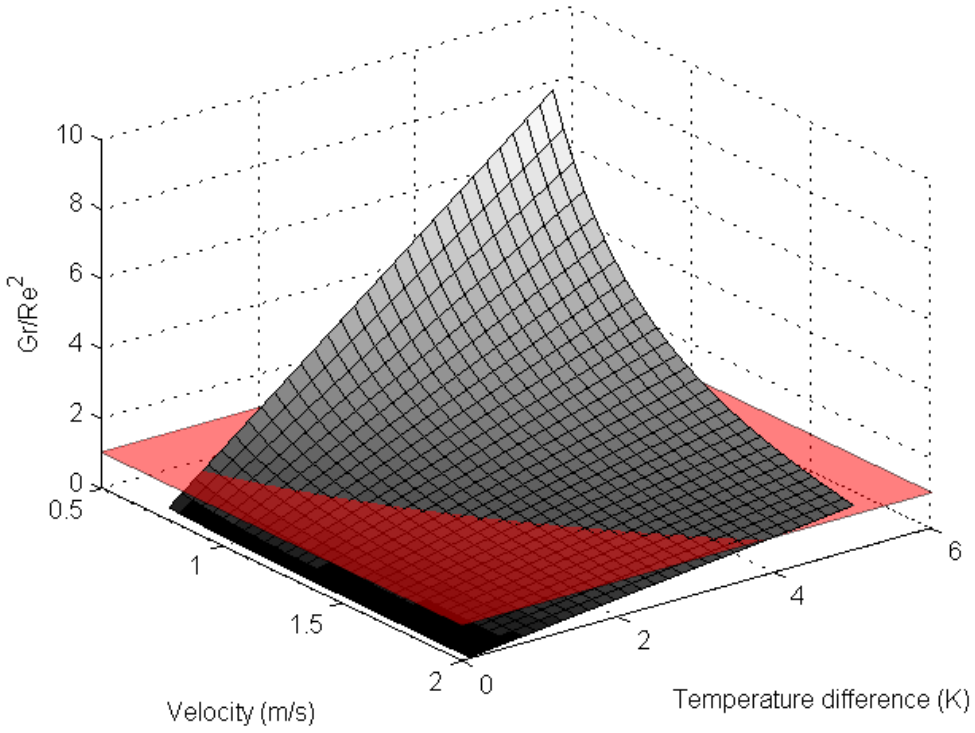

Figure 20. Ratio of Grashof number to the square of Reynolds number as a function of velocity and temperature difference. Values above one correspond to natural convection dominated flow.

Judging from the figure, it is clear that the forced convection requires specific conditions to be fulfilled prior to becoming the dominant flow type, but it is quite challenging to reliably estimate the actual velocity and temperature difference values without any measurements. However, this approach can be used to roughly estimate the effect of varying temperatures and velocities on the dominating flow type. Naturally, the aspect ratio of the tank also affects to the forming of natural convection, and this is not taken into account with this model as the characteristic length was chosen freely. Some estimations were also done to assess the effect of characteristic length (i.e. swapping velocity or temperature difference with characteristic length and producing similar figures), but its influence was found to be considerably smaller than that of velocity and temperature difference in this case. In conclusion, it seems bit more unlikely for the forced flow to dominate the tank, but nevertheless it was considered as one possible outcome for simulation purposes.

Realistically the flow is a mixture of both, and the dynamic nature of the feeding process could actually contribute to a sudden reversal of the dominating flow type, as was observed in the preliminary simulations done for this thesis.

Source term in the momentum equation is given in ANSYS Fluent as N/m^3. Thus a rough value for the momentum source can be derived from the Boussinesq approximation

$$(\rho - \rho_o)g \approx -\rho_o \beta (\mathrm{T} - \mathrm{T_o})g \tag{18}$$

where ρ_0 is the reference density (bulk average density), and T_o the corresponding temperature. The Boussinesq approximation can be used to assess buoyancy effects in fluids in terms of a single density and temperature differences.

According to equation (18), the momentum brought to the liquid is roughly 14.4 N/m^3 per degree Kelvin. If we expect the temperature difference to lie somewhere in the region of three degrees, the momentum would be roughly 50 N/m^3, which was actually chosen as the momentum condition for simulation cases. The three degrees was observed as a typical temperature difference between the surface and the tank floor in the preliminary simulations. In hindsight, the value for the momentum source should have been higher to show any real variation in the results, and the three-degree estimation was rather low. A summary of the chosen values for the desublimation model is given in section 3.8.

3.6.4 Evaporation-condensation

Evaporation was implemented by using a UDF (introduced in section 3.4.4.), which required only the time relaxation parameter as an input value. The coefficient was fixed to a value of 0.02, which seemed to be a fairly good estimate of the BOR. Other values were derived automatically from the computed solution. Unlike the desublimation model, the evaporation-condensation model is not restricted by location, which means that evaporation could occur even below the liquid surface if conditions are suitable. The model is based on the temperature difference between the computational cell and the saturation temperature in that cell. The saturation temperature is derived from the pressure of the cell by using a correlation which was introduced in section 3.5.2.

3.6.5 Computational settings

The remaining initial values and computational settings have been collected to table 5.

Table 5. Additional computational settings

Evaporation-condensation model coefficient	0.02
Heat exchange model between phases	Ranz-Marshall
Gravity	on
Turbulence model	Standard k-ε
Wall function	Standard wall function
Pressure-velocity coupling	Phase-coupled SIMPLE
Discretization	2nd order upwind, geo-construct scheme
Transient formulation	First order implicit
Drag coefficient between phases	Symmetry law
Operating pressure	Fixed / floating operating pressure (depending on case)

3.7 Mesh

A structured 2D axisymmetric grid with quadrilateral cells is used. The tank is assumed to be a flat-bottomed cylinder, and the injection of the carbon dioxide is implemented into the middle portion of the tank. Typically the natural gas inlet feeds are located near the tank walls so it would be natural if the CO_2 inlet would as well be located there, but that approach would require a more complex 3D simulation which was deemed to be out scope of this thesis. By focusing on the 2D case, more detailed attention can be directed towards the modelling of the boil-off and carbon dioxide desublimation process.

Mesh was refined in two specific areas: the injection point of carbon dioxide and the fluid-vapour interface (i.e. liquid surface). Mesh was generated using ANSYS ICEM CFD 15.0. In total, the computational grid included roughly 43000 nodes.

During the simulations multiple revisions were required for the mesh as problematic regions and phenomena were observed. In the final mesh the wanted y+ value was fixed to a value of roughly 50 by using cell distances of 0.004 … 0.15 m. The exceptionally large variation

is caused by the two phases, which have substantially different densities. The final revision of the mesh is presented in figure 21. Even with the multiple revisions the current mesh experienced some issues in the simulations. Further discussion about mesh is conducted in chapter 4.

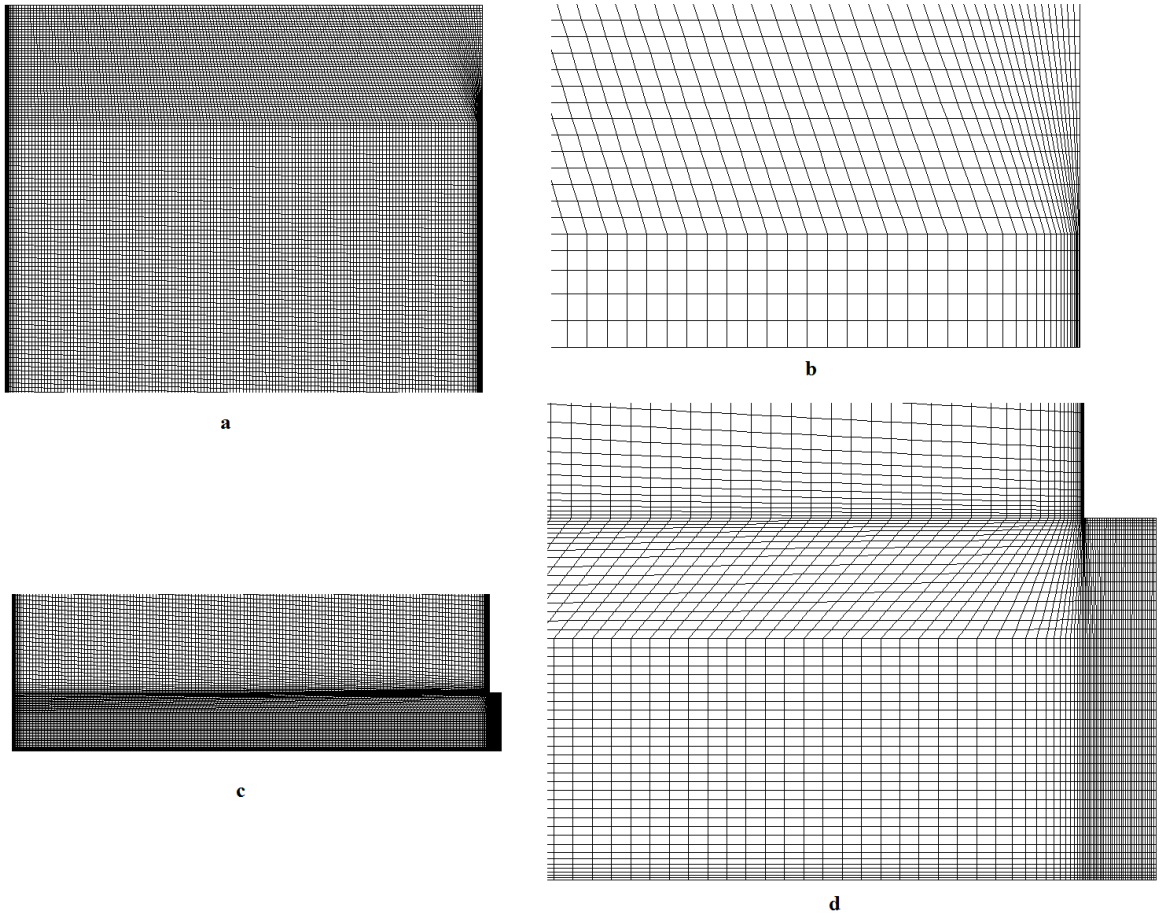

Figure 21. Upper section of the mesh (a), zoomed in section of the liquid-vapour interface in upper section (b), lower portion of the mesh (c), details of the inlet region in lower portion of the tank (d).

3.8 Simulations

The simulations in this thesis have been divided into two sections: simulation series 1 and 2. Series 2 is the main focus of this thesis, with three distinct cases. Initially the series included one extra case designed to showcase a larger momentum condition, but it was left out of the final results due to unrealistic flow conditions. In its stead, the results from an earlier simulation from series 1 is used. Table 6 shows the main differences of the two simulation series.

Table 6. Main differences of the two simulation series.

	Simulation series 1	Simulation series 2
Pressure	Fixed	Floating operating pressure
Material densities	Temperature-dependent	Real gas model (vapour), constant with Boussinesq approximation (liquid)
Mesh	Refined near liquid-vapour interface	No refinement in the interface region
Precision	Single precision	Double precision

Each simulation series was initially started without CO_2 feeding, so only the heat leaks from the tank walls contributed to the boil-off gas generation and flow pattern formation. In this thesis, the term *preliminary simulation* is used to refer to this period. After the tank had been given some time to settle, the carbon dioxide feed-in process was initiated using various parameters in the different simulation cases, and the boil-off rate was compared to the preliminary solution. In addition, the flow behaviour was observed.

One justification for using this *preliminary simulation* before the initiation of the CO_2 feeding process is that in seasonal storage operation such a tank is likely to remain relatively idle for longer periods, during which the internal flows are dictated by the heat leaks into the tank. Additionally, this approach improves the initial computational stability of the later simulations. Figure 22 presents an overview of the simulations, and table 7 lists the parameters of the main simulation cases. The conditions and parameters of the additional tests are mentioned separately when they are introduced.

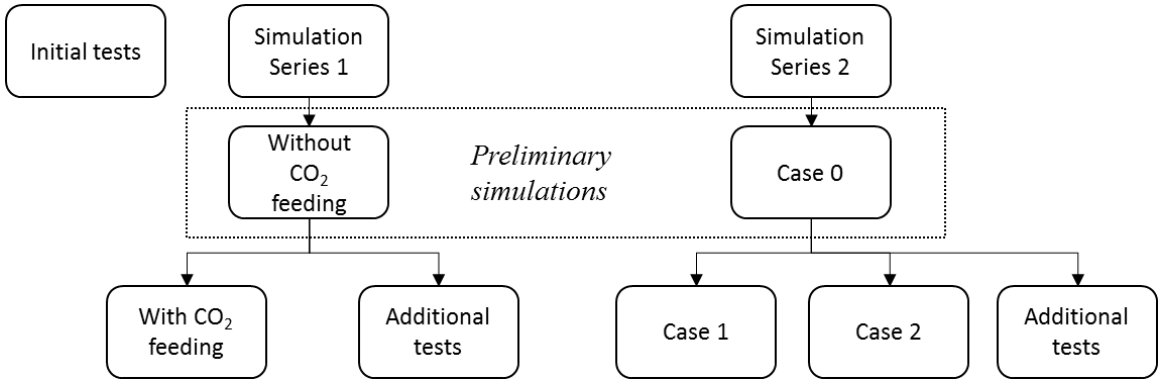

Figure 22. An overview of the different simulations conducted in this thesis.

Table 7. Conditions for the simulation cases.

	CO_2 feed condition %	Momentum condition N/m^3
Case 0	0	0
Case 1	25	50
Case 2	50	50

4 RESULTS

In this chapter, the results and observations from the simulations are presented. As an introduction, general issues and observations from the simulation are given, followed by the results from the simulations regarding the flow patterns and boil-off. As was introduced in section 3.8., the simulations are divided into two series, and the latter series had three distinctly numbered cases.

4.1 General observations and issues

This section addresses the issues that arouse during the simulations. The two simulation series (see section 3.8.) are compared, as the behaviour and results of these simulations were in some cases radically different.

4.1.1 Time step size

The time step size in time-marching calculations is restricted by the Courant–Friedrichs–Lewy (CFL) condition, which links solution stability (or specifically flow velocities) to a dimensionless number called the Courant number. It is dependent on the time step size, cell size and flow velocity, and in explicit solvers its maximum allowable value is generally 1. The maximum desired Courant number could be defined in ANSYS Fluent. Depending on the current state of the simulation, the maximum Courant number was defined somewhere between 0.2 – 1 in these simulations.

A variable time step was used in the simulations. The very first initial tests were run with a freely changing time step size, but later on this approach was modified so that a maximum value for the time step size was defined. The maximum allowed time step size varied between simulation cases from 0.04 to 0.12 seconds. This approach stabilized the solution noticeably, as the velocities in the tank no longer portrayed as heavy fluctuation as before. Without the defined maximum time step size, vapour space flow velocities increased substantially (even to unrealistic proportions), which in turn caused the time step to decrease

to a region of 0.0001 seconds. This was often connected to the poor convergence of a time step, causing the velocities of the next time step to deviate noticeably. Especially the edges (both physical wall edges and the liquid-vapour interface) of the domain were vulnerable to this type of behaviour.

During normal simulations, the Courant number typically lowered down to values close to or below 0.2, as the time step size was not restricted by the Courant number but rather by the maximum time step size. This resulted in a slightly longer computational time, but it was still considered preferable to a larger time step with potential flow instabilities. However, when the CO_2 feeding process was initialized, Courant number typically rose and became the limiting factor. One of the most likely reasons for this behaviour was caused by the mesh, which is discussed in the next section.

4.1.2 Mesh

Many of the encountered simulation issues were connected to the computational grid, and especially the wall sections of the domain. The computational mesh was revised multiple times during and between the calculations, but even still some issues remained. To clarify some of the issues, two different mesh types are highlighted in this chapter: one with a heavily refined region near the liquid-vapour interface, and one with no refinement in that region (these correspond to simulation series 1 and 2, respectively). Initially the refined mesh was used, but due to computational settings used in that simulation the liquid level rapidly decreased, causing the refined region to be left completely to bulk vapour region. This had undesired effects on simulation stability and computational time, and it was therefore agreed that an unrefined mesh should also be tested. This had some effect on the evaporation rate at the liquid interface, as is discussed in section 4.1.4.

There were also multiple smaller differences between those meshes and multiple sub revisions under each mesh type, but the comparison of those is not very beneficial. One of the benefits of the different revisions was that a larger time step could be used in the simulation as the problematic regions were identified and fixed.

One issue in the simulations that was not completely eliminated was caused by the wall regions of the tank. Due to the nature of the problem, flow conditions near the wall changed radically during the simulations. During the preliminary operation, velocities near the wall are generally below 0.1 m/s, but the CO_2 feeding process could locally increase the velocity nearly hundredfold and simultaneously cause the y+ value to shift from the optimal region. Additionally, the two phases required different wall distances to achieve the desired y^+ values, and poorly chosen cell distances especially in the interface between two regions caused instability in the solution. This was observed as single cells or cell clusters having exceptionally high velocities near the wall region in some instances. Locally, the y+ values could rise up to 3000 during the simulations.

In hindsight, the roof construction should have been made in a parabolic form instead of a rectangular. Parabolic construction gives a more realistic representation of a real tank [73], and with a well-designed mesh the heavy vortex forming and turbulence could be minimized in that region. However, most of the issues experienced during the simulations were caused by the liquid phase of the domain so the benefit of such a construction is not crucial.

4.1.3 Mass balance

In this section, it is important to remember that the two simulation series had differently configured pressure conditions. Series 1 included a fixed operating pressure, whereas series 2 had a floating operating pressure, which allowed the gradual increase of pressure inside the tank.

It was observed during the simulations that the total mass of the tank decreases with a fixed operating pressure. This in turn caused the liquid level to decrease at a rate of 360 mm per hour, when according to thermodynamic energy balance the liquid level should have decreased at a rate of roughly 0.3 mm per hour. As was mentioned in the previous section, this caused the refined region to lie completely in the vapour section of the domain, which considereably slowed the calculations.

This type of mass loss is unrealistic, but unfortunately a conclusive reason could not be found for this phenomenon. It should be noted that in all simulations the volumes of the both phases

coincided (i.e. if liquid volume decreased, vapour volume increased by the same amount). This caused some confusion in data processing, as initially only the volumes of the phases were tracked. When this mass loss was finally observed, further simulation tests were carried out.

It was found out in tests with series 1 that the mass transfer between the phases was a major contributor to the unrealistic mass loss in the tank. It seemed like the mass transfer had been based on purely volume variations between the phases, which would mean that the density difference between the phases would correspond to the missing mass. However, even when the mass transfer between phases had been disabled, there was still some mass imbalance observed. Presumably this may also be somehow linked to the fixed operating pressure, as the pressure remained unphysically constant during these tests.

Another potential contributor is the used precision, as the total mass of the tank is quite large ($2.8 \cdot 10^7$ kg) and with the single precision solver the last included digit represents kilograms, whereas in double precision the last digit represents nanograms in this case. This phenomenon affects especially the data gathering process, which may have been a crucial factor when performing the various tests in series 1 as the time span of the tests was considerably small (often less than a minute).

In a realistic situation, pressure inside the tank will increase, which will also have an effect on the BOR. Eventually the generated BOG will have to be ejected through the pressure relief valves. The simulation series 2 enabled this gradual increase of pressure inside the tank, along with other different configurations shown earlier in section 3.8. After some initial instabilities, the mass in the tank settled to a constant value as seen in figure 23 . The reason for the initial variance is hard to pinpoint, but one possible reason is unstable residuals - although the absolute values of the residuals were well below 10^{-12} even during the initial stage. Even so, the final residuals decreased linearly as the simulation progressed, and fluctuations during the iteration sequences were less common.

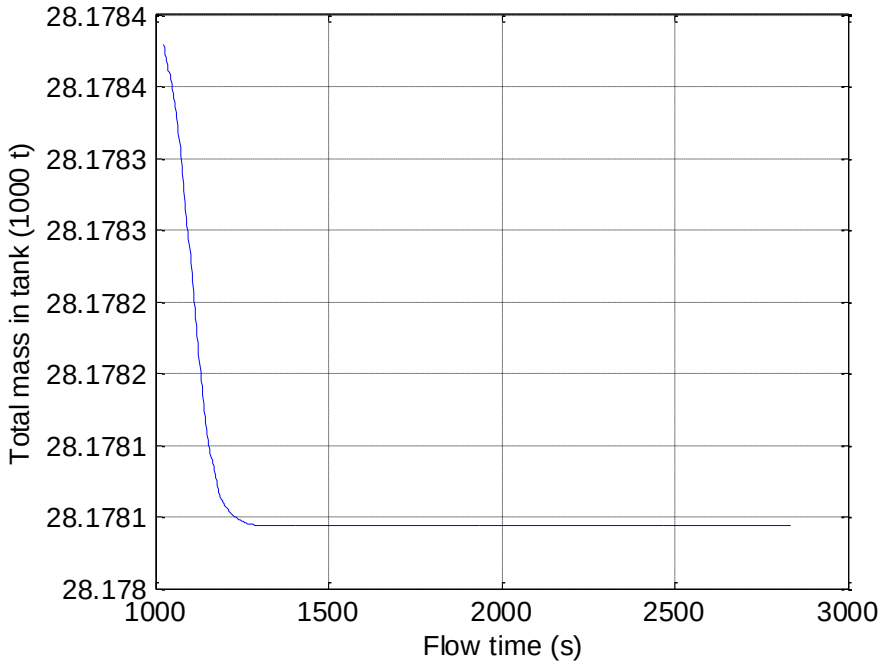

Figure 23. Total mass in tank in case 0. Total mass decreases about 300 kg before settling on the final value. The total mass of the tank decreases 0.02 ‰.

Additionally, if the UDF for mass transfer was the only reason for the mass loss, its effects should be visible also at and after the 1500 s mark, which is not the case. This leads to conclusion that the mass evacuation could be a combination of different reasons. As the mass loss is quite limited compared to the total mass of the tank, this phenomenon can be presumed to have little effect on the results. To summarize the observations done to this point, the preliminary simulation in series 2 lost some mass from the tank in the very beginning, but stabilized later. The series 1 demonstrated a more radical rate of mass loss, and it continued throughout the simulation.

Figure 24 presents a scenario, where the CO_2 feeding has been initialized at time 1635 s (this marks the starting point of cases 1 and 2). The source terms for the momentum and energy icrease linearly until they reach their maximum values at time 1735 s. As can be seen from the figure, total mass in the tank started to decrease after a certain time. As the time step size simultaneously dropped (i.e. convergence worsened), it may be possible that there are some interferences in the calculations. Similar results were observed in all the simulation cases of series 2 with CO_2 feeding enabled.

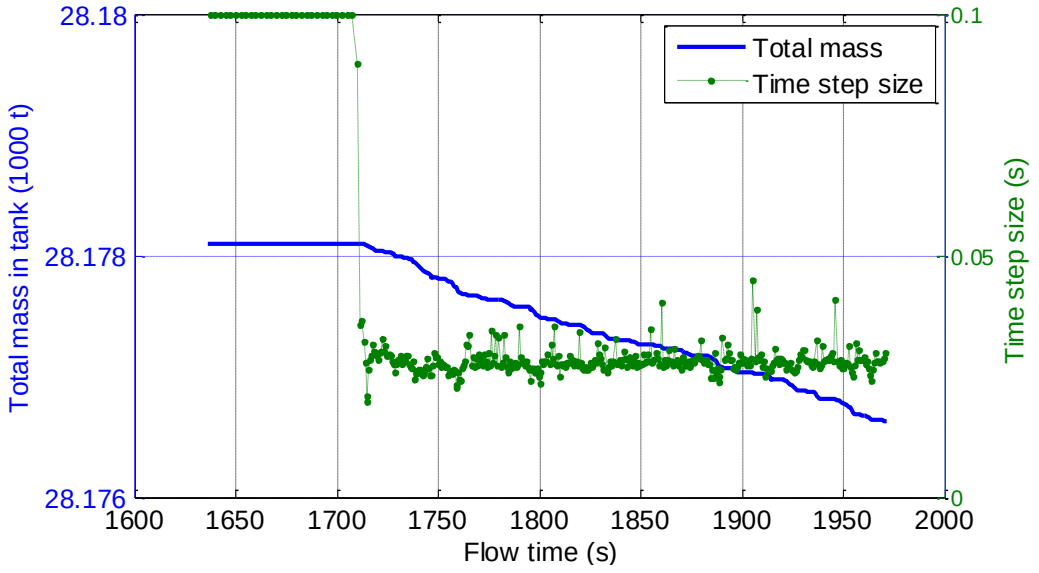

Figure 24. Total mass in tank and time step size when CO_2 feeding is initialized (case 1). Mass is not conserved after the 1700 s mark.

The pressure which was tracked during the simulations was the absolute maximum pressure inside the tank, which also included the effect of hydrostatic pressure. With mass being lost in the tank, it also affects the hydrostatic pressure and likely causes some additional noise in the data. As can be seen from the pressure diagram in figure 25, the pressure was generally on an increasing trend. This could be seen even more clearly if the data had been collected with time averaging over multiple timesteps. The data gathering in these simulations was done every 25th timestep without any averaging, which results in a time interval of roughly 0.5 … 3 seconds.

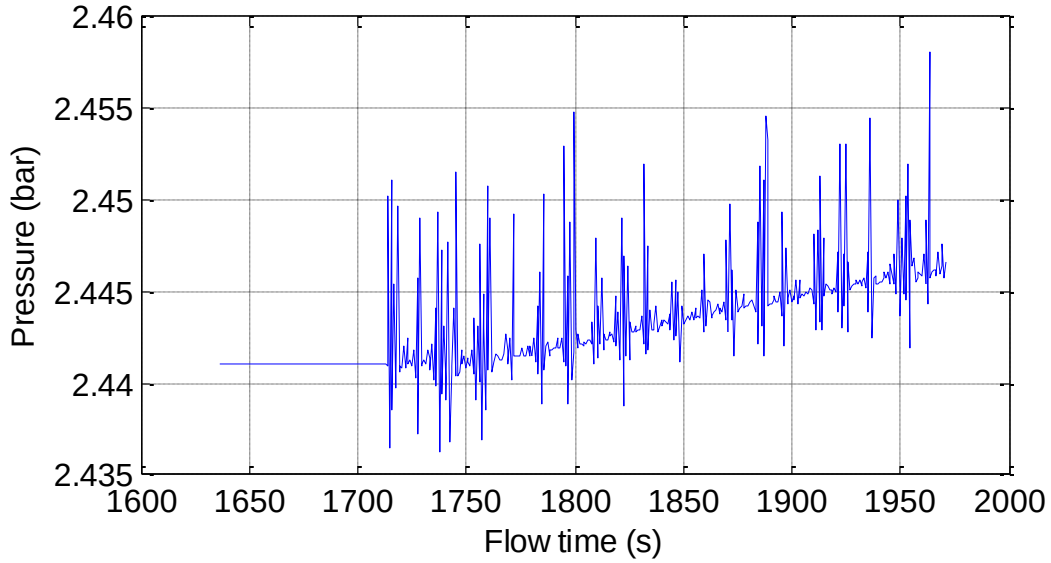

Figure 25. Maximum pressure inside the tank in case 1. After the CO2 feeding has been initialized, some fluctuation is observed in the pressure.

4.1.4 Evaporation-condensation

The evaporation-condensation model included a time relaxation coefficient, which had to be manually adjusted by using an up-and-down method. The final value was fixed to 0.02 for both the evaporation and condensation. This was justified on the basis that during the *preliminary simulation* the only contributing factors to BOR are the heat leaks into the container, and with the chosen coefficient the BOR was roughly in agreement with the theoretical heat leak calculations. The coefficient was fixed while running the *preliminary simulation* of series 1 (i.e. with fixed operation pressure), and figure 26 presents the BOR during the later stages of that simulation.

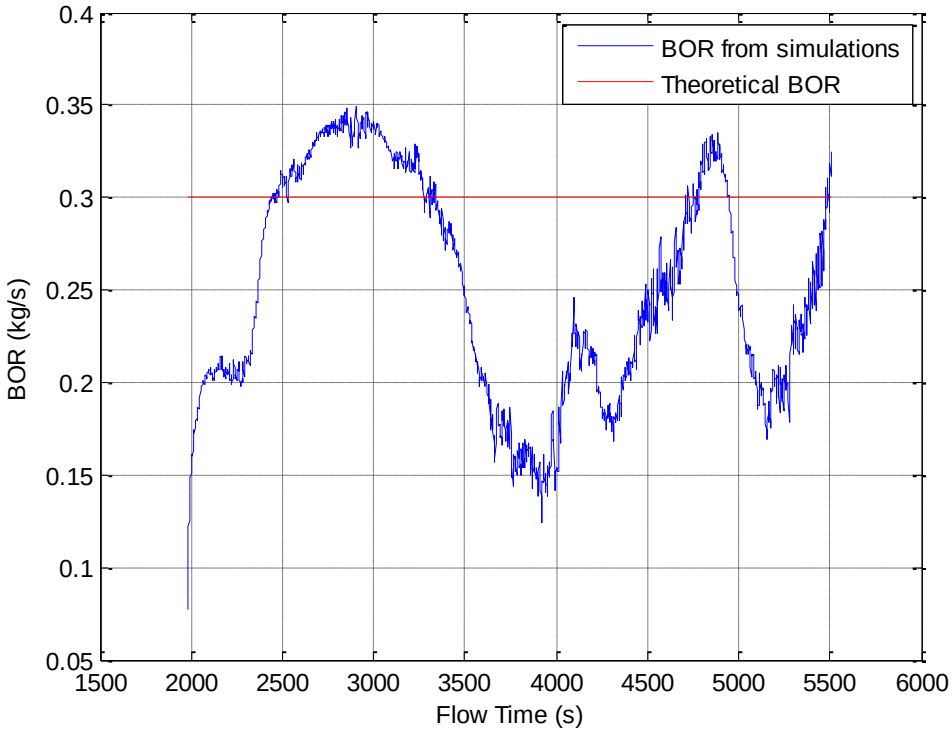

Figure 26. Boil-off rate during simulation with a fixed operation pressure (series 1 preliminary simulation).

With the floating operating pressure (series 2), the BOG decreased with time as seen in figure 27. Natural reason for this behaviour is the gradual increase in the pressure: as pressure increases, the saturation temperature increases as well, and thus BOR decreases. Eventually the saturation temperature exceeded the temperature of the fluid at the surface, and the BOG generation almost halted completely.

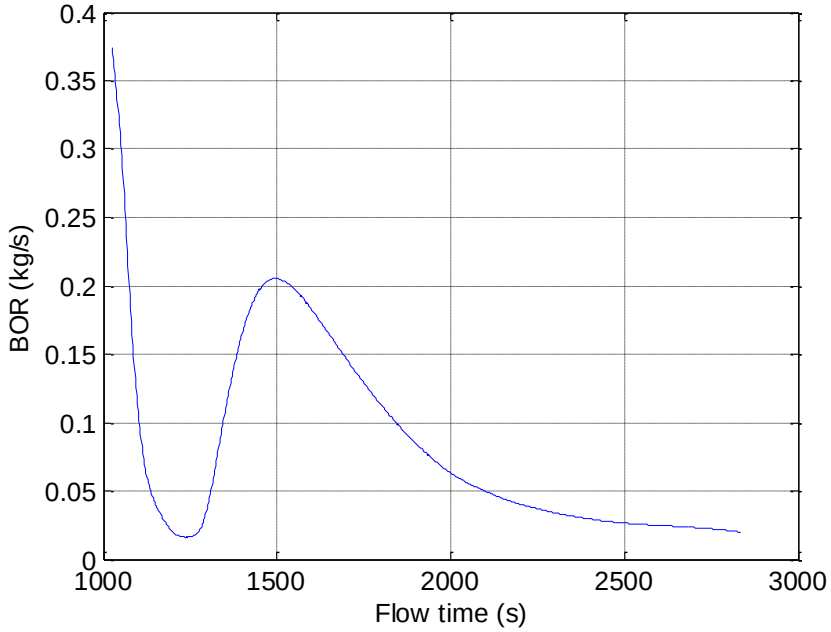

Figure 27. Boil-off rate with a floating operating pressure (case 0). After the initial spike, BOR asymptotically approaches zero.

The deviation of saturation temperature is quite small (e.g. when the pressure increases 1000 Pa, saturation temperature increases roughly 0.1 K). The effect is still enough to make a devastating difference. In total the pressure increased in the tank less than 3000 Pa, which is still a relatively small amount. If the bulk temperature of the liquid had been initialized slightly higher, BOG generation would have continued slightly longer but eventually the result would be the same. Figure 28 shows the final state of the liquid-vapour interface: the topmost liquid cell is at the saturation temperature, and BOR is nearly zero.

Based on these results, it is possible that the fixed value for the evaporation coefficient is flawed. Since the first simulation series was done with the fixed operation pressure, the only actual variable affecting the situation is the temperature at the interface. If the bulk temperature of the liquid is slightly above the saturation temperature (which it was), the coefficient is not actually fixed to represent the boil off due to heat leaks into the container, but rather a certain portion of the liquid which is transferred to the surface. Naturally, this is somewhat dependent on the heat leaks as natural convection is the driving force pushing warmer liquid onto the surface, but still some additional verifications should be conducted.

In the floating operating pressure simulation type (series 2), BOG generation halts because the coefficient is not large enough to properly display the effects of heat leaks, and the bulk liquid is no longer warmer than the saturation temperature. If the coefficient would be larger, it could be possible that the system becomes sensitive enough to properly model the effects of heat leaks into the tank. Another potential contributor to this can be the large cell size near the interface.

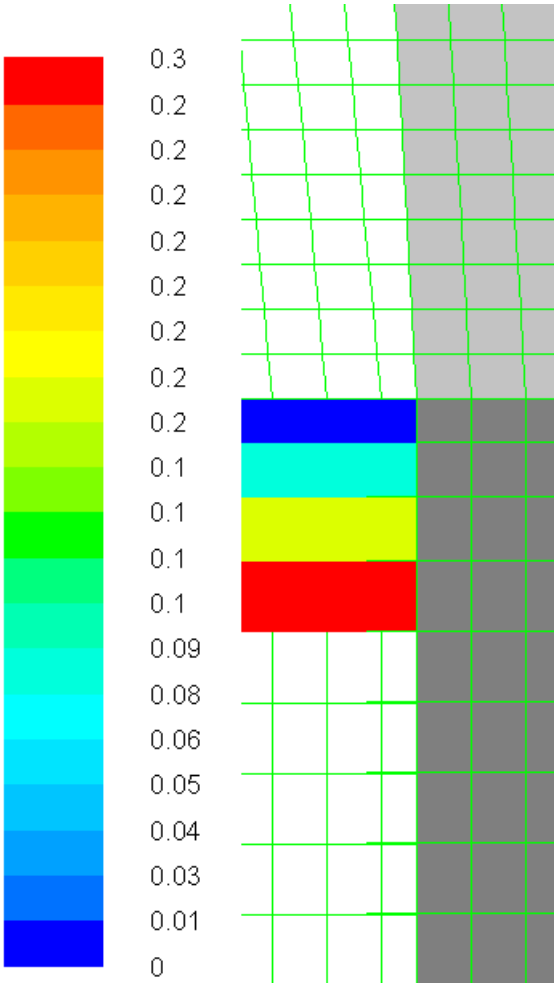

Figure 28. Cell temperature compared to saturation temperature and phase boundary in case 0. The light and dark gray on the right hand side correspond to vapor and liquid phase, respectively. The colored tiles represent the temperature difference between cell temperature and saturation temperature.

When the temperature of the cell is precisely at the saturation temperature, the UDF was defined so that the condensation from the vapour phase occurs. However, as we recall from

equation (9), the mass transfer is calculated using vapour density which is roughly 200 times smaller than that of liquid phase. Thus the actual mass transferred between phases is negligible. This leaves the system in a very delicate oscillating motion between evaporation and condensation, which is barely noticeable. As a final remark, the boil-off rate changes if the mesh is refined in the interface. Thus the evaporation coefficient is somewhat dependent on the mesh, although this has not been verified extensively.

4.1.5 Turbulence viscosity ratio

One issue during the simulations was the high turbulent viscosity ratio. Turbulent viscosity ratio is defined simply as the ratio between turbulent and laminar viscosity. Practically as soon the solution was initialized, turbulence viscosity ratio started to increase rapidly, until it reached the maximum cut-off value, which is defined in ANSYS Fluent. However, in some simulations the viscosity ratio also decreased after being restricted to the maximum for some time. One possible explanation for the large turbulence viscosity ratio is the poor grid and problems caused by it. The initial area where the ratio started to increase heavily seemed to be located in the liquid-vapour interface, as can be deduced from figure 29.

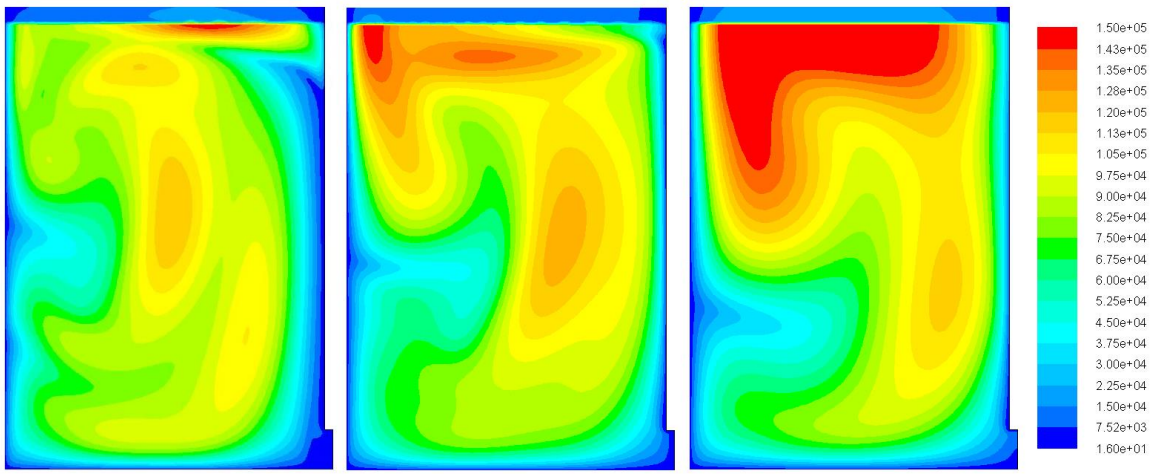

Figure 29. The evolution of turbulent viscosity ratio in simulation case 0.

4.2 Flow regimes

This section addresses the flow behaviour in the tank. The section has been divided into two parts: one for the *preliminary simulation* without CO_2 feeding, and another with the CO_2 feeding enabled.

4.2.1 Preliminary study without CO_2 feeding

Figure 30 shows the fluid flow velocities with respect to tank height from three different radial locations. The three chosen radial locations are at 0.8 m, 12 m and 24.8 m, which correspond to the CO_2 inlet vicinity, the radial midpoint of the tank and the tank wall vicinity, respectively. A 20 cm gap has been left between the locations and the actual physical barriers. All of the data presented in this section is from the *preliminary simulation* of series 1, but the corresponding data from series 2 is nearly identical.

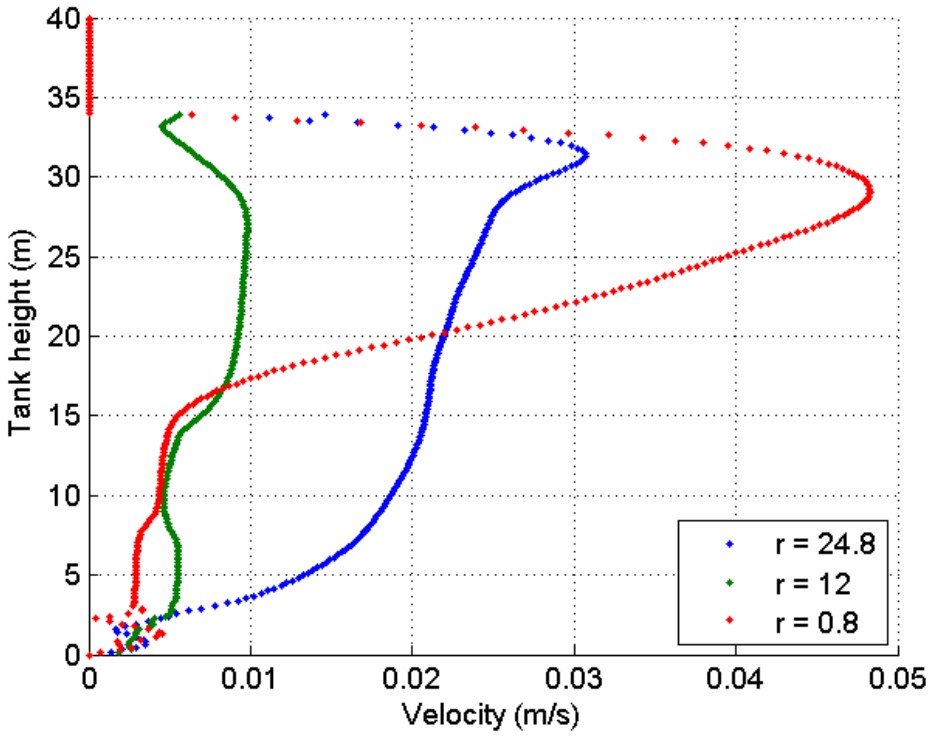

Figure 30. Liquid velocity from three different radial sections: wall vicinity (blue), radial middlesection (green) and CO_2 inlet region (red). Data from preliminary simulation of series 1.

During the preliminary operation without CO_2 feeding, liquid located near the wall of the tank heats up due to the heat leaks through the construction, which causes the liquid to drift

upward. Velocities are moderate, and an approximate time for a liquid particle travelling with the flow to transfer to the top is in the range of 30-60 minutes. Once the flow reaches the surface, there is a slight increase in the local velocity as the liquid travels towards the centre of the tank. In the middle section of the tank, a potent downward-flowing stream forms as can be seen from the graph corresponding to radial distance of 0.8 m. Flow is slightly turbulent near the tank floor, which is mainly caused by the heat transfer through the tank floor. Flow velocity is zero after the 34 m mark, because at that point the vapour phase begins and only the liquid velocities are shown. The described flow pattern matches well with the one found from the literature (introduced in section 3.1.3.).

Figure 31 shows the velocites from three different height levels, which are 4 m, 20 m and 33.5 m. The radial coordinate 0 is fixed at the tank centre. Liquid level height was initially at 34 meters. Velocities show a gradual increase towards the top of the tank, and velocities are largest in the vicinity of the the edges, as can be expected due to the presence of the convective flow. Wave patterns can also be observed in the figure, which implies that small vertical jets form in the tank. This can also be confirmed from the velocity and temperature contours.

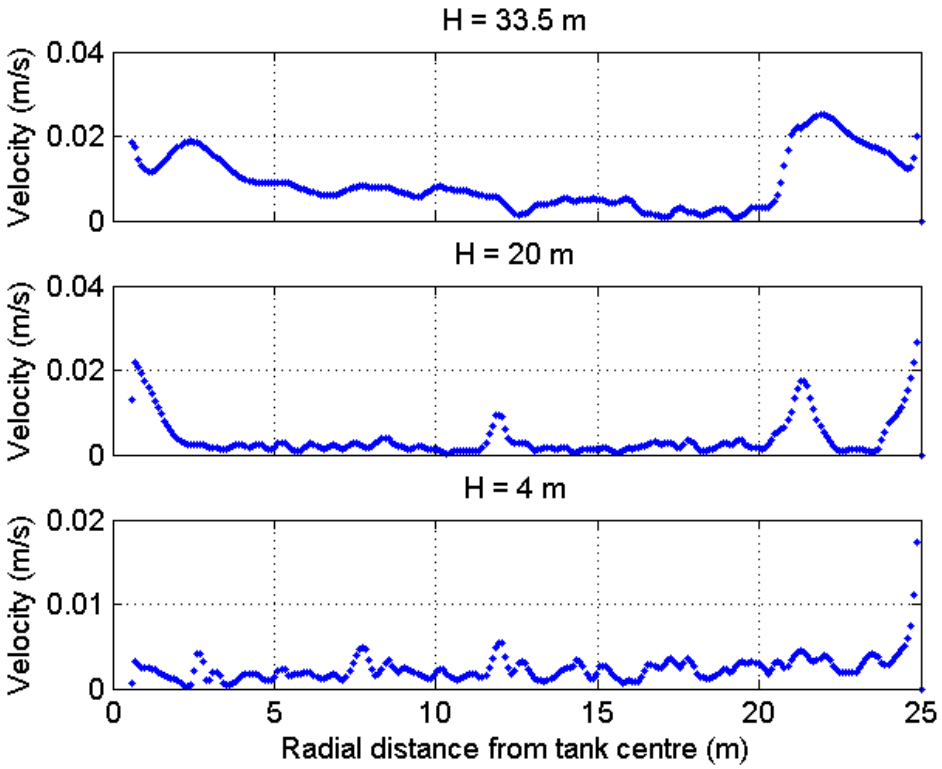

Figure 31. Liquid velocity at three different height levels: below the liquid-vapor interface, middle section of the tank and above the CO_2 inlet.

As simulation was continued, the velocity profiles deviated significantly from the previous figures 30 and 31. As a comparison, figure 32 depicts the corresponding velocity profiles at a later time (approximately 30 minutes later). The wavy patterns are more dominant and the velocity variations caused by the vertical jets can be seen more clearly in the figures from the later simulation.

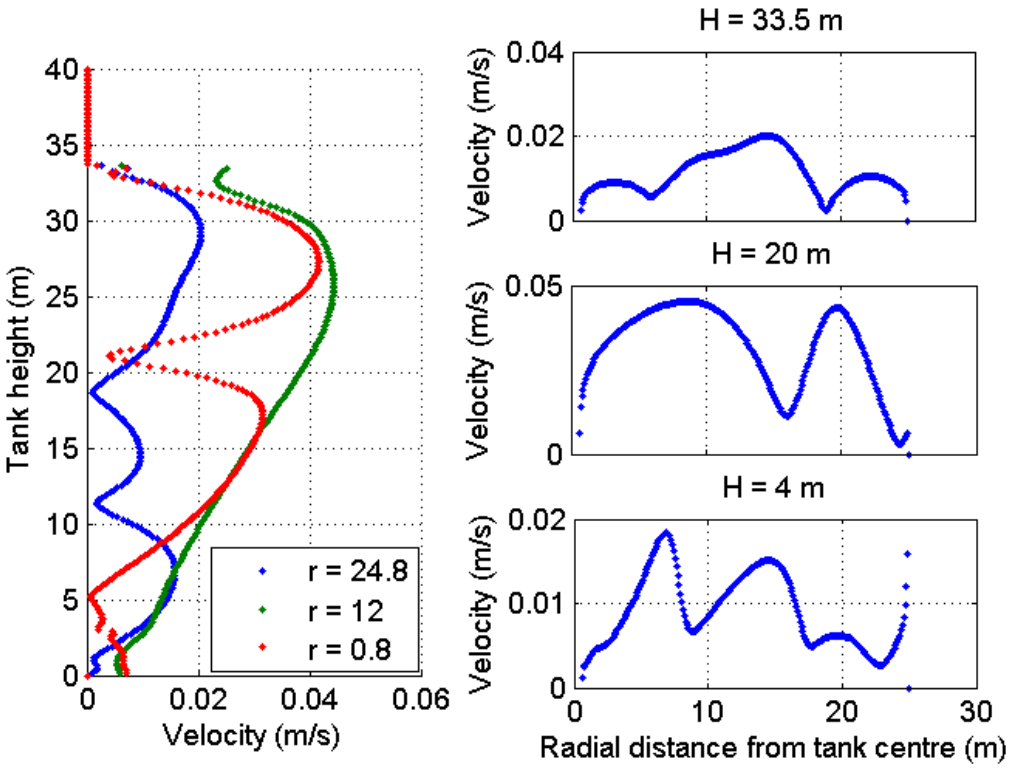

Figure 32. Liquid velocities at a later time.

Figure 33 shows a vector diagram of the velocities at a later time. The flow has changed so that the flow near the vertical wall has switched direction, so it now travels down towards the tank floor whereas before the flow travelled upwards. The reason for this seems to be the heat transferred through the tank flooring, as it overpowers the heat transfer occurring near the wall. This also causes a potent swirling flow in the tank. Further verification should be conducted on how the heat leaks distribute among different wall sections, as evidently this has a relatively large impact on the flow patterns.

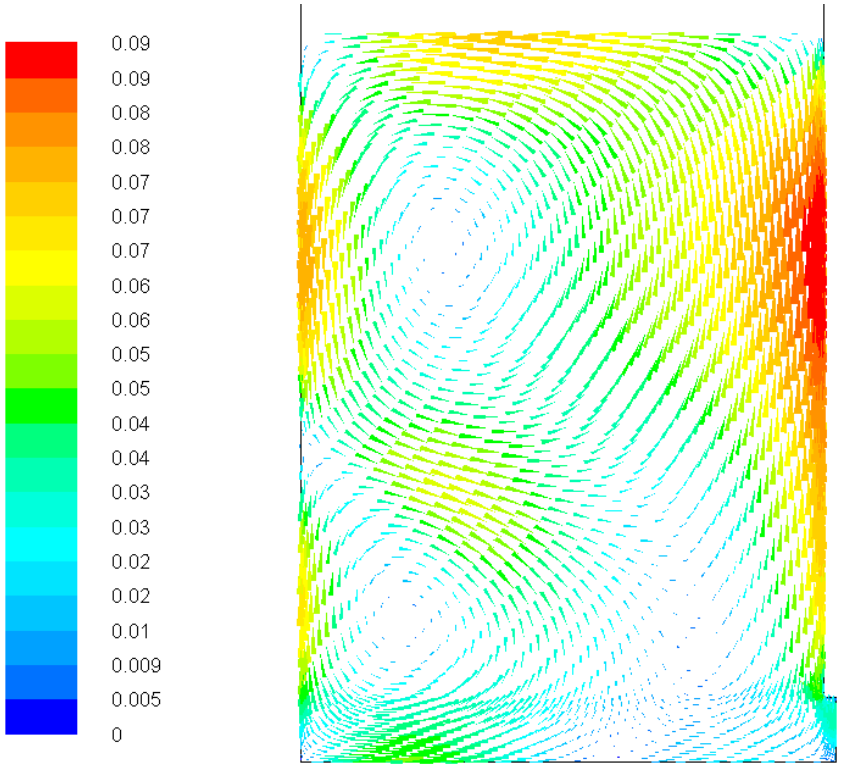

Figure 33. Flow velocity (m/s) as a vector field without CO_2 feeding.

4.2.2 With CO_2 feeding

Figure 34 shows the velocities with 25 % CO_2 feeding enabled (case 1). The case 2 with a 50 % feed condition is similar, with slightly larger velocities at the wall section. The velocities are clearly larger near the inlet pipe, where the liquid is rising up due to the desublimation reaction warming the liquid. Transfer time to the top is now only about 1-2 minutes.

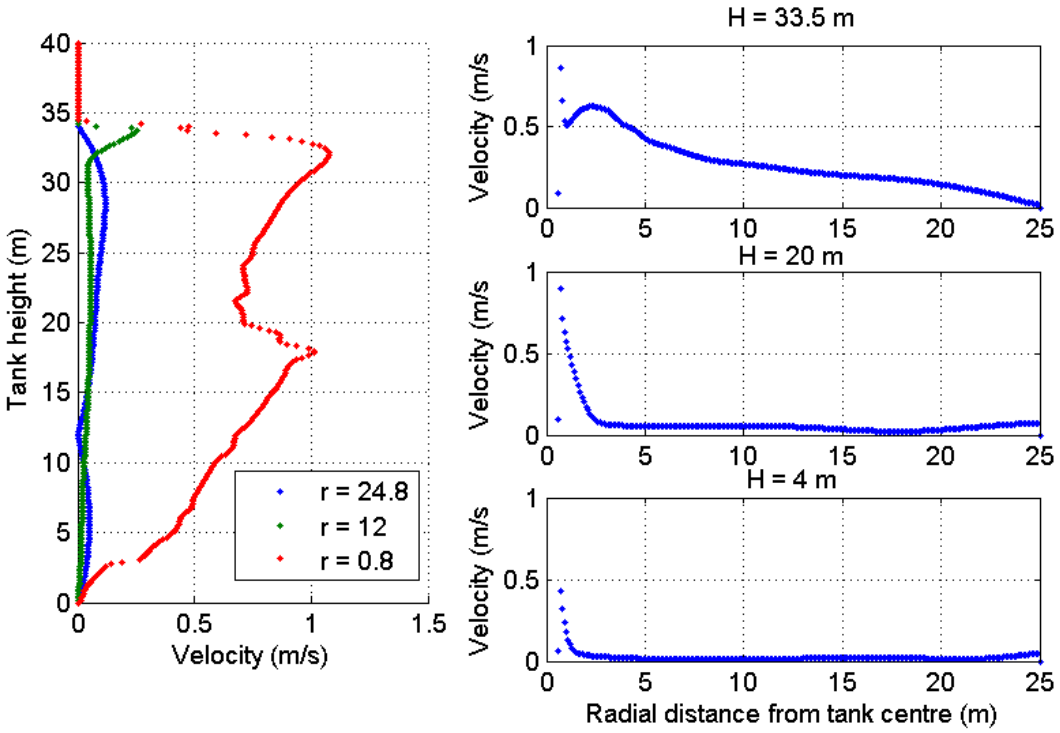

Figure 34. Velocity distributions in tank with CO_2 feeding enabled (case 1).

Figure 35 presents the flow velocity as a vector field in two distinct cases. On the left is a snapshot of a test with a momentum source term defined as 700 N/m^3 (simulation from series 1). This case represents the momentum-dominated flow. In this simulation the momentum source term causes the flow to hit the tank floor, from where it curls up and rises near the inlet pipe. On the right side of the figure is case 1, which represents the buoyancy dominated flow. Momentum source term was defined as 50 N/m^3. In this case, the heat source term causes the flow to travel straight up beside the inlet pipe, even though the momentum source is defined in the opposite direction in the desublimation region.

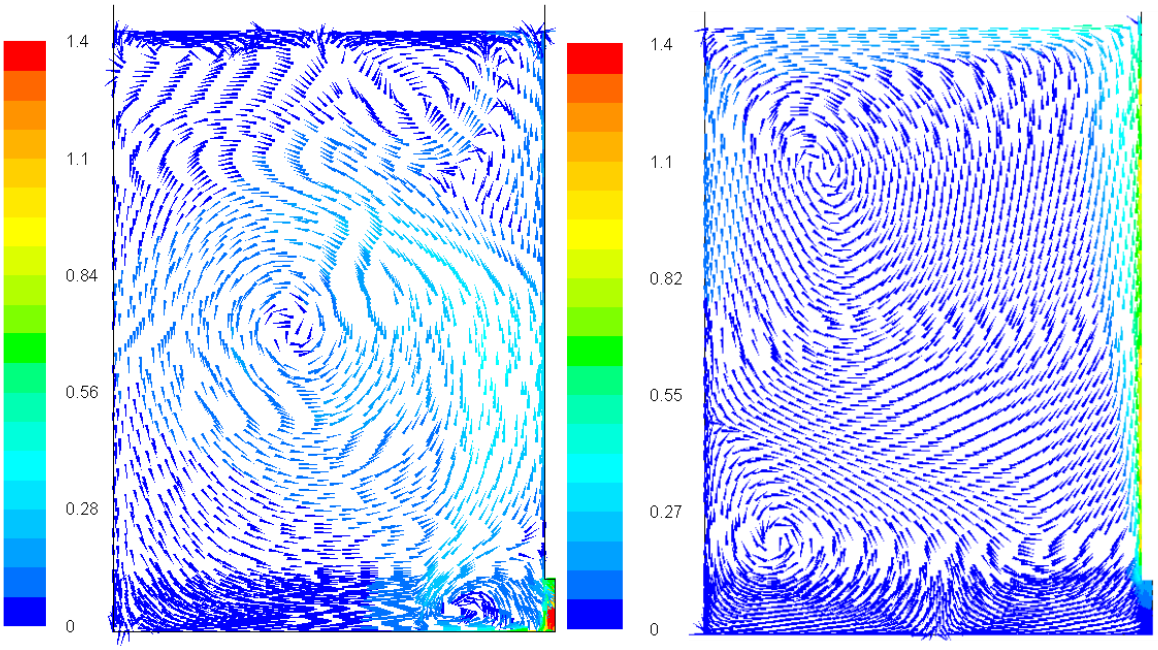

Figure 35. Flow patterns in the tank described with vector fields. The arrows are colored by velocity, with a unit of m/s. Left hand side shows a momentum-dominated flow, while the right hand side is from case 1 which is dominated by natural convection.

The maximum temperature (of single cells) in the inlet region increased substantially as the CO_2 feed was initiated. The evolution of these temperatures can be seen in figure 36. The maximum temperature actually rises above the saturation temperature in the inlet region. The total maximum pressure (including the hydrostatic pressure) inside the tank was roughly 2.4 bars, which corresponds to a saturation temperature of 123 K. As the maximum temperature is in both cases 1 and 2 multiple degrees above that, evaporation could occur within the liquid. However, the volume-averaged temperatures in the inlet region still remain below the saturation temperature. It was observed from the simulations, that the highest temperatures are located close to the wall which resembles the pipe inlet, and it seemed like a portion of the liquid was unable to escape the region. This could cause the temperatures to rise to higher levels than in a realistic situation. Naturally, the temperatures are heavily dependent on the magnitude of the energy and momentum source terms, but nevertheless these results show that below-surface evaporation cannot be conclusively dismissed as impossible.

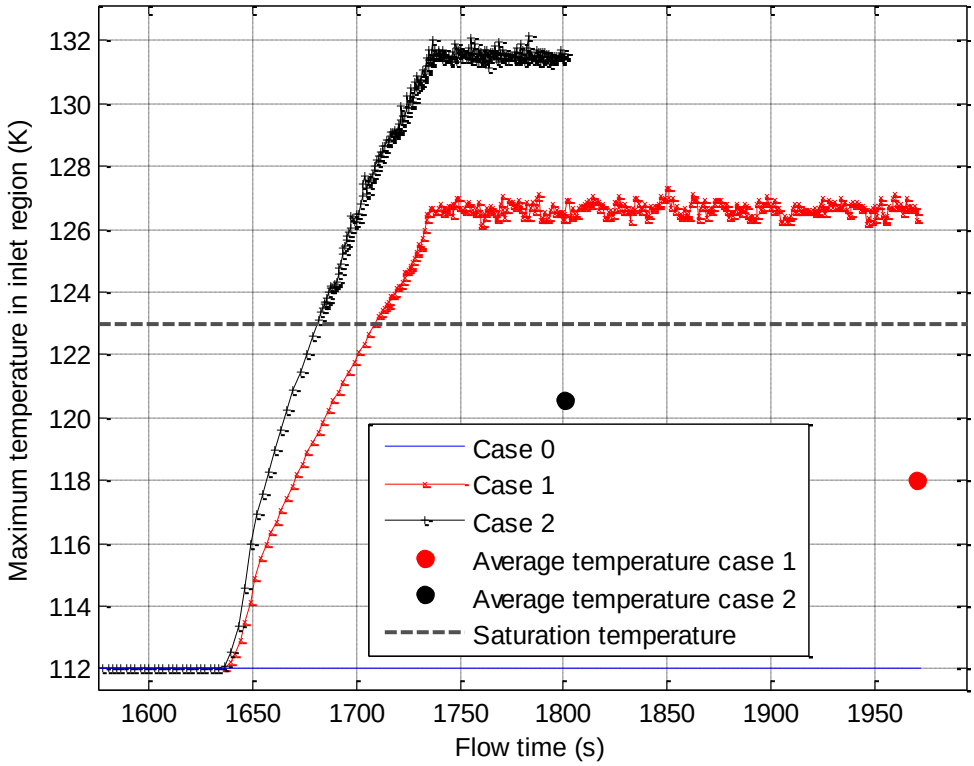

Figure 36. Maximum temperature in the inlet region in various simulation cases, with an estimation of the saturation temperature in that region. Also the volume-averaged temperatures for a single time step are shown.

Evaporation was disabled in the inlet region (i.e. the same region which includes the momentum and energy source terms), so that tracked boil-off rate would not be influenced by the below-surface evaporation. All other regions of the tank were eligible for evaporation, but the surface was the only region with actual evaporation occurring.

When compared to rollover observed in conventional LNG tanks, CO_2 feeding could potentially be either harmful or beneficial. On one hand, the CO_2 desublimation causes the liquid to warm up, which is the primary reason for the eventual rollover occurrence. On the other hand, the process of warming up the liquid seems to be much faster than that caused by heat leaks into the tank. Thus the flow induced by CO_2 feeding could actually cause existing stratified layers to break up. Modelling of this subject may be problematic as many different conditions need to be considered.

4.3 Boil-off

Boil off rates in the simulations with floating operating pressure are presented in figure 37. According to the thermodynamic energy balance, the BOR rates should be 0.3, 4.3 and 8.2 kg/s in cases 0, 1 and 2 respectively. Clearly, the values given by the simulation are much smaller. The second case demonstrated numerical instability, and eventually the simulation was discontinued. One potential contributor is the computational mesh. With the larger energy source term, the velocities in the vicinity of the inlet pipe increased, which in turn caused the y+ values to increase to larger values than in the other simulation cases. Another important observation that can be done from the figure is that the time delay between initiating the CO_2 feeding process and observing a change in the BOR is around 2 minutes. This observation is supported by the earlier estimations done with the flow velocities.

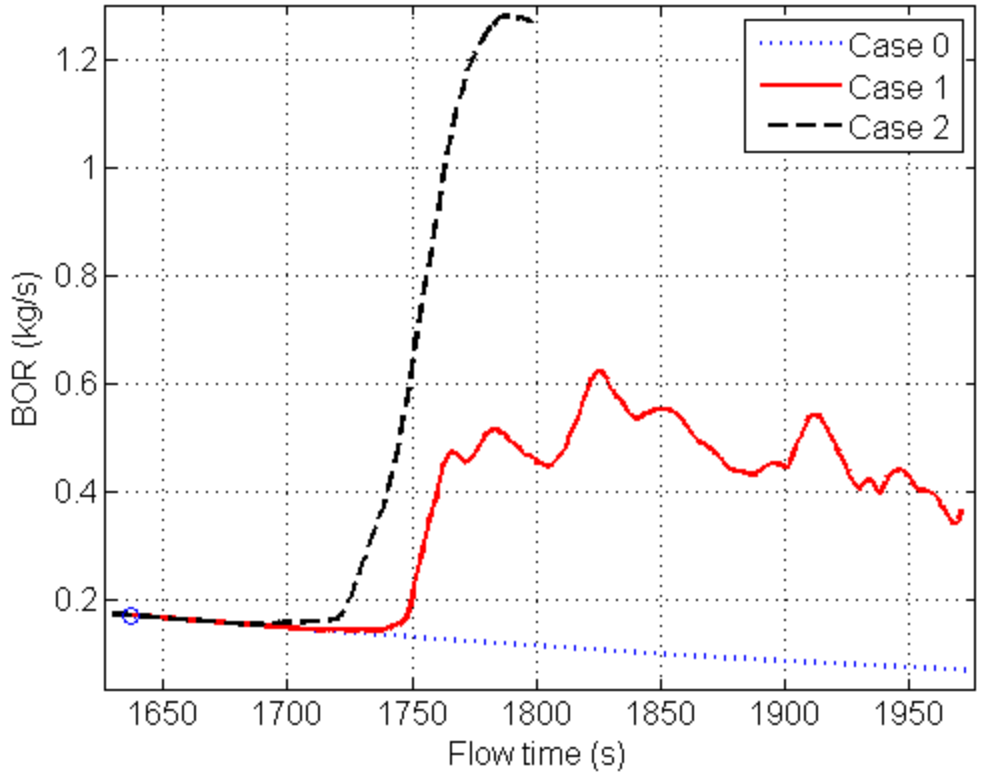

Figure 37. BOR in simulation cases 0, 1 and 2. CO_2 feed time initialization has been marked with a circle. Case 2 simulation was discontinued as numerical instability was observed in the results.

The thermodynamic energy balance evaluation is based on the assumption that pressure inside the tank does not change. The three cases presented in figure 37 were all done with a

floating operating pressure, which could be one reason for the lower BOR. Another possible reason is that the value for the evaporation coefficient used in the model was chosen incorrectly. Simulation conditions were not exactly the same when the value for the coefficient was derived and when the actual simulation cases were run. Computational mesh and pressure settings were changed in between, which both contribute to the BOR.

One short simulation experiment was also done with a pressure outlet condition, but this simulation suffered from rapid mass loss from the tank. The rate was measured to be roughly 2000 kilograms per second, which is quite large even with the huge scale of the tank. On the other hand, the simulation was not carried out for a longer time period, and it could be possible that the situation stabilizes with time. The boil-off rate during the test was roughly 0.15 kilograms per second, which is roughly half of the rate given by the thermodynamic balance. This could mean that the pressurization indeed affects the derived BOR, but still there is some additional error in the derivation.

It can be concluded that the current model did not appropriately model the boil-off phenomenon. Simulations with a floating operating pressure had significantly lower mass loss rate from the tank, but lacked in the accurate representation of the BOR. Simulations with pressure outlet condition or fixed pressure had a more realistic value for the BOR, but conversely suffered from serious mass loss within the tank. One aspect that should be studied is that does the mass loss decrease after considerable time when using a pressure outlet condition, as this type of simulation is clearly the best alternative considering long-term simulations. Furthermore, an estimation of the ratio between mass evacuated through the outlet and mass outright disappearing within the tank could give further insight into the issue. Floating operating pressure simulations could possibly work with a shorter timespan if the evaporation coefficient is fixed to an alternative value, but at some point the BOR is guaranteed to decrease as the pressure inside the tank increases. Nevertheless the evaporation coefficient used in this thesis should not be taken as granted, but tested and fine-tuned in further simulations.

5 CONCLUSIONS

The model developed in this thesis included two major components, a desublimation model and an evaporation-condensation model. The desublimation model did not actually model the carbon dioxide as a physical substance, but rather as an energy and momentum source term in a given location of the tank.

The desublimation model is useful in assessing the flow patterns when CO_2 is fed to the different locations of the tank. In this task the model functions well, although some manual labour is required to separate the desublimation region from the rest of the domain. Further development of this model component would likely require some statistical data of the desublimation reaction. For instance, the current model predicted that it may be possible for the cryogenic liquid to reach boiling conditions below the liquid surface as a result of the desublimation phenomenon, but this result relies heavily on assumptions about the volume of the desublimation region. It would therefore be critical to measure how large domain of influence the desublimation reaction has when the carbon dioxide is inserted into the tank.

The momentum source term of the desublimation model had little effect on the flow patterns inside the tank. Natural convection dominated the simulations, unless the source term was defined to be very large, which could almost be defined as manipulation of the results. Naturally some crude assumptions were made in this context, and one key question concerning this subject is how much of the momentum from the gas particles is transferred into the liquid, as this could be taken into account when evaluating the magnitude of the momentum source term.

Variation of the desublimation model heat source term did have a significant effect on the flow velocity magnitude in the tank, but the flow patterns varied quite little overall. The current model probably does not give an accurate presentation of the inlet region, as the mixing of the different phases and the phase change reactions were not included. Backflow into the inlet pipe is one potentially dangerous phenomenon, as desublimation inside the pipe could cause the pipe to clog up or rupture. This is especially important if the pipe is

submerged, as the hydrostatic pressure could cause the liquid to rise up along the pipe walls during downtime periods.

The evaporation-condensation model, which was used to evaluate the boil-off rate in the tank, did not match well with the rate derived from the thermodynamic energy balance. There are a few explanations to this. Firstly, the evaporation model has a coefficient, which is used to fine-tune the evaporation rate. With further experimentation, a more suitable value could be found for the coefficient. Secondly, the pressure inside the tank heavily influences the boil-off rate. Simulations with a fixed pressure (i.e. when pressure effects are not considered) matched better with the thermodynamic energy balance calculations, but there was still a significant difference. Thirdly, the computational mesh influences the boil-off rate. In conclusion, these factors caused the predicted boil-off rate to differ from the theoretical rate, but otherwise the model was applicable.

One of the most curious phenomena observed in this thesis was the mass loss from the tank. The UDF-implemented evaporation-condensation model seems like a good candidate for being the driving force for this type of behaviour, but then it would be reasonable to assume that this type of behaviour would be consistent. However, in some instances it was observed that the total mass was preserved even though the evaporation process continued. It therefore seems more likely that instabilities in the simulation, or a combination of different reasons caused this type of behaviour. In most cases the mass loss rate was so low that it could be dismissed, but especially the early sections of the simulations often suffered from higher loss rates. Simulations with a fixed pressure or a pressure outlet condition had a significantly larger mass loss rate, compared to simulations with a floating operating pressure.

In the current simulation the liquid was assumed to be homogenous, and with these conditions the liquid flow quickly rose up to the surface along the inlet pipe. Thus no direct link could be found between the CO_2 injection and the formation of stratified layers in the tank, although the model is inadequate to properly evaluate this threat. The buoyant flow induced by the CO_2 injection is likely to be much stronger than that caused by the heat leaks into the tank, but the exact effect of this to the stratification phenomena is hard to predict

accurately. In this context, alternative ways to feed the carbon dioxide into the storage tank should also be considered.

Integrating a power plant to the system is a crucial part of the energy storage concept. The thermodynamic evaluation performed in this thesis revealed that if the flue gases are directed into the storage tank with cryogenic liquid, it is likely that the amount of flue gases fed needs to be limited. Otherwise more hydrocarbons are removed from the tank than could be handled by the combustion plant. This would require an intermediate storage, or an external sink such as a natural gas network.

According to the conducted simulations there is no large time delay between initiating carbon dioxide feeding and observing a change in the boil-off rate at the surface. This would suggest that carbon dioxide tank could not be used as some sort of buffer to absorb thermal energy and release it gradually, at least with the current configuration.

Considering future development, it is important to verify that this type of integrated storage offers some clear benefit over the separated storage of the individual components, and that a cyclic process with a decent overall efficiency can be constructed in general. Furthermore, a reliable system for the feeding and removal of CO_2 is one of the major challenges. Despite these challenges, it seems that there will be a strong market for energy storage concepts in the future, and power-to-gas solutions have the benefit of having existing infrastructure and mature technology. Especially the large-scale benefits of these systems are an undeniable asset when compared to other alternative technologies. Natural gas grids, the transportation sector and energy production are all important sections of our society, and power-to-gas solutions may easily be integrated with each of those.

6 SUMMARY

The role of energy storage concepts is becoming more important in the future as the share of intermittent energy production increases. Power-to-gas technologies hold great potential for future energy storage transformation, largely thanks to the existing infrastructure and the large field of applications. Possibly in a longer timescale gas-based technologies will see a trend shifting from fossil-fuel based gas industry to synthetically manufactured gases, but this could be seen as a possibility rather than a threat.

The integrated storage tank investigated in this thesis is designed to simultaneously contain both carbon dioxide and cryogenic liquefied hydrocarbons, such as LNG. Flue gases from an oxy-fuel combustion plant could be fed into the tank, where the carbon dioxide would desublimate in direct contact with the cryogenic liquid. Later the stored carbon dioxide could be converted into synthetic methane by using an electrolysis-methanation process, and then combusted again to form a closed loop for carbon.

As the main objective, this thesis investigated the effects of feeding carbon dioxide into a cryogenic tank containing methane. The developed CFD model included two major components: a desublimation model and an evaporation-condensation model. The desublimation model can be used to evaluate the large scale flows inside the tank that arise from the desublimation reaction. The evaporation-condensation model is useful in estimating the hydrocarbon evaporation rate from the tank, which is caused by the heat leaks from the ambient environment and the thermal energy contained in the flue gases.

The desublimation phenomenon between liquids and gases was identified as one of the most critical aspects that requires additional research and measurements for further model development. The dynamic handling of the flue gases may be problematic, as the processing capacity of the power plant is easily exceeded. The time delay between flue gas feeding and observing a change in boil-off rate is quite minimal, which would mean that the storage tank could not be used as a buffer storage. One solution to this problem is to use natural gas grid as a sink for the excess evaporated hydrocarbons. A more detailed dynamic study containing the different components (e.g. electrolyser, boiler) should also be conducted.

REFERENCES

1 Lux Research Inc. Grid Storage under the Microscope: Using Local Knowledge to Forecast Global Demand. 2012.

2 European Commission. Energy roadmap 2050. 2012. Retrieved 1.8.2014 from: https://ec.europa.eu/energy/sites/ener/files/documents/2012_energy_roadmap_2050_en_0.pdf

3 European Electricity Grid initiative (EEGI), Grid+. Energy Storage Innovation in Europe: A mapping exercise. 2013.

4 European network of transmission system operators for gas (ENTSOG). Ten-Year Network Development Plan 2013-2022. 2013.

5 European Commission. DG ENER Working Paper: The future role and challenges of Energy Storage. 2013.

6 European association for storage of energy (EASE), European energy research alliance (EERA). European energy storage technology development roadmap towards 2030: Technical annex. 2013.

7 European Commission, Eurostat. 2014. Total gross electricity generation (ten00087), Primary production of renewable energy by type (ten00081). Retrieved 6.8.2014 from: http://ec.europa.eu/eurostat/web/energy/data/main-tables

8 European power exchange. Market data, day-ahead auction. Retrieved 6.8.2014 from: https://www.epexspot.com/en/market-data

9 Energypost, Simona Benedettini and Carlo Stagnaro. The case for allowing negative electricity prices. May 27, 2014. Retrieved 5.8.2014 from: http://www.energypost.eu/case-allowing-negative-electricity-prices/

10 National renewable energy laboratory (NREL). Melaina, M. W., Antonia, O., Penev, M. Blending Hydrogen into Natural Gas Pipeline Networks: A Review of Key Issues. 2013

11 Kirk-Othmer Encyclopedia of Chemical Technology: Fuels, Synthetic, Gaseous Fuels. 2000. John Wiley & Sons Inc.

12 Bauer, F., Persson, T., Hulteberg, C., Tamm, D. Biogas upgrading - technology overview, comparision and perspectives for the future. 2013. Biofuels Bioproducts & Biorefining (Biofpr).

13 Gas Infrastructure Europe (GIE). LNG Investment Database. Retrieved 7.8.2014 from: http://www.gie.eu/index.php/maps-data/lng-investment-database

14 European network of transmission system operators for gas (ENTSOG), Gas Infrastructure Europe (GIE). System development map 2012.

15 Gas Infrastructure Europe (GIE). GSE Storage map. Retrieved 7.8.2014 from: http://www.gie.eu/index.php/maps-data/gse-storage-map

16 European Association for Storage of Energy (EASE). Energy storage technologies. Retrieved 7.8.2014 from: http://www.ease-storage.eu/technologies.html

17 Tusiani, M., Shearer, G. LNG: A Nontechnical Guide. 2007. PennWell.

18 European Standard EN 1160. Installation and equipment for liquefied natural gas - General characteristics of liquefied natural gas. 1996.

19 International Energy Agency (IEA). Energy Supply Security 2014. Part 1.

20 Cryogenic Fuels, Inc. Liquid Methane Fuel Characterization and Safety Assessment Report. 1991.

21 U.S Energy Information Administration. Annual Energy Outlook 2014 Early Release Overview.
22 International Energy Agency (IEA). Medium-Term Gas Market Report 2014.
23 Depail, J-C, Gas Infrastructure Europe. Presentation: Gas infrastructure and security of supply. 2014. Retrieved 27.7.2014 from: http://www.gie.eu/index.php/publications/cat_view/3-gle-publications
24 Moran, M.J., Shapiro, H.N. Fundamentals of Engineering Thermodynamics. 2002. John Wiley & Sons Ltd.
25 Toftegaard, M.B, Brix, J., Jensen, P.A., Glarborg, P., Jensen, A.D. Oxy-fuel combustion of solid fuels. 2010. Progress in Energy and Combustion science 36, 581-625.
26 Kvamsdal, H.M., Jordal, K., Bolland, O. A quantative comparison of gas turbine cycles with CO2 capture. 2007. Energy 32 10-24.
27 De Falco, M., Iaquaniello, G., Centi, G. CO2: A Valuable Source of Carbon. 2013. Green Energy and Technology. Springer-Verlag London
28 National Institute of Standards and Technology (NIST). Chemistry WebBook. Thermophysical Properties of Fluid Systems. Retrieved 9.1.2015 from: http://webbook.nist.gov/chemistry/
29 Rath, S., Krol, M. Comparative Risk Assessment for Different LNG-Storage Tank Concepts. 2013. Chemical Engineering Transactions 31.
30 Young-myung Yang, Korea Gas Corporation. Developement of the world's largest above-ground full containment LNG storage tank. 2006. 23rd World Gas Conference.
31 Lun, H. Filippone, F. Roger, D.C., Poser, M. Design and construction aspects of post-tensioned LNG storage tanks in Europe and Australasia
32 LNG World News. Picture of The Day: First QCLNG Tank Hydro-Test by BG. Retrieved 31.12.2014 from: http://www.lngworldnews.com/picture-of-the-day-first-qclng-tank-hydro-test-by-bg/
33 European Standard EN 1473. Installation and equipment for liquefied natural gas. Design of onshore installations
34 Inco Nickel. Advertisement poster. 9% Nickel steel wins giant hammer test at -320°F. 1961
35 Furuya, H. et. Al. Nippon Steel and Sumitomo Metal Corporation. Development of low-nickel steel for LNG storage tanks. 2013. LNG 17 International Conference & Exhibition on Liqufied Natural Gas Proceedings.
36 Nippon Steel & Sumitomo Metal. NSSMC's 7% Ni Steel for LNG Storage Tank will be Used to Build the LNG Storage Tank for Imported Shale Gas form Canada. 2014. Retrieved 2.1.2015 from http://www.nssmc.com/en/news/20140619_100.html
37 Kramer, E., Kellaris, N., Daal, M., Sadoulet, B., Golwala, S., Hollister, M. Material selection for Cryogenic Support Structures. 2014. Journal of Low Temperature Physics 176 (1103-1108)
38 Adorjan, A. S. Heat transfer in LNG engineering. 1991. Hemisphere, cop.
39 Timmerhaus, K. D., Reed, R. P. Cryogenic Engineering: Fifty Years of Progress. 2007. Springer.
40 Fornasiero, G. R. LNG Tank Foundation Heating Parameters. 1986. Advances in Cryogenic Engineering 31 (1141-1149).
41 European Standard EN 14620. Design and manufacture of site built, vertical, cylindrical, flat-bottomed steel tanks for the storage of refrigerated, liquefied gases with operating temperatures between 0°C and -165°C.

42 Bates, S., Morrison, D. S. Modelling the behaviour of stratified liquid natural gas in storage tanks: a study of the rollover phenomenon. 1996. International Journal of Heat and Mass Transfer 40 (1875-1884)
43 Woodward, J. L., Pitblado, R. M. LNG Risk Based Safety Modelling and Consequence Analysis. 2010. John Wiley & Sons.
44 European Standard EN 1160. Installations and equipment for liquefied natural gas. General characteristics of liquefied natural gas.
45 Arjomandnia, P., Tade M.O., Pareek, V., May, E.F. Analysis of Available Data from Liquefied Natural Gas Rollover Incidents to Determine Critical Stability Ratios. 2013. AlChE 60 (362-374)
46 Deshpande, K. B., Zimmerman, W. B., Tennant, M. T., Webster, M. B., Lukaszewski, M.W. Optimization methods for the real-time inverse problem posed by modelling of liquefied natural gas storage. 2011. Chemical Engineering Journal 170 (44-52).
47 Koyama, K, Tokyo Gas Co. CFD Simulation on LNG Storage Tank to Improve Safety, Efficiency and Reduce Cost. 2008. International Gas Union Research Conference (IGRC).
48 Lukaszewski, M.W., Zimmerman, W.B.J., Tennant, M.T., Webster, M.B. Application of inverse methods based algorithms to Liqufied Natural Gas (LNG) storage management. 2013. Chemical engineering research and design 91 (457-463).
49 Zimmerman, W.B., Rees, J.M. Rollover instability due to double diffusion in a stably stratified cylindrical tank. 2007. Physics of fluids 19.
50 Rama Subba Reddy Gorla. Rapid calculation procedure to determine the pressurizing period for stored cryogenic fluids. 2010. Applied Thermal Engineering.
51 Ebenezer Adom, Sheikh Zahidul Islam, Xianda Ji. Modelling of Boil-Off Gas in LNG Tanks: A Case Study. 2010. International Journal of Engineering and Technology 2 (292-296)
52 Zmohamad Shukri Zakaria, Kahar Osman, Mohd Noor Asril Saadun, Muhammad Zaidan abd Manaf, Mohd Hafidzal Mohd Hanafi. Computational Simulation of Boil-Off Gas Formation inside Liquefied natural Gas tank using Evaporation Model in ANSYS Fluent. 2013. Applied Mechanics and Material 393 (839-844).
53 Zellouf, Y., Portannier, B. First step in optimizing LNG storages for offshore terminals. 2011. Journal of Natural Gas Science and Engineering 3 (582-590).
54 E. Querol, B. Gonzalez-Regueral, J. García-Torrent, M.J. García-Martínez. Boil off gas (BOG) management in Spanish liquid natural gas (LNG) terminals. 2010. Applied Energy 87 (3384-3392).
55 Chansaem Park, Kiwook Song, Sangho Lee, Youngsub Lim, Chonghun Han. Retrofit design of a boil-off gas handling process in liquefied natural gas receiving terminals. 2012 Energy 44 (69-78).
56 Dimopoulos, G.G., Frangopoulos, C.A. A Dynamic Model for Liquefied Natural Gas Evaporation During Marine Transportation. 2008. Int. J. of Thermodynamics 11 (123-131).
57 Zellouf, Y., GDF SUEZ. LNG Master®: Safe and optimized storage despite LNG diversity. 2010. 16th International Conference and Exhibition on Liquefied Natural Gas.
58 V. A. Naletov, V. L. Lukyanov, N. N. Kulov, A. Yu. Naletov, and M. B. Glebov. An Experimental Study of Desublimation of Carbon Dioxide from a Gas Mixture. 2013. Theoretical Foundations of Chemical Engineering. 48 (312-319)
59 Marek Henczka, Jerzy Bałdyga, Boris Yu. Shekunov. Modelling of spray-freezing with compressed carbon dioxide. 2006. Chemical Engineering Science 61. (2880-2887)
60 Al-Hakim, K., Wigley, G., Stapley, A.G.F. Phase doppler anemometry studies of spray freezing. 2006. Chemical Engineering Research and Design 84 (1142-1151).

61 C. Anandharamakrishnan , J. Gimbun , A. G. F. Stapley & C. D. Rielly (2009) Application of Computational Fluid Dynamics (CFD) Simulations to Spray-Freezing Operations, Drying Technology: An International Journal, 28:1, 94-102
62 V. A. Naletov, L. S. Gordeev, M. B. Glebov, and A. Yu. Naletov. Mathematical Modeling of Desublimation of Carbon Dioxide from Flue Gases of Heat Power Systems. 2013. Theoretical Foundations of Chemical Engineering 48 (27-33).
63 Chun-Feng Song, Yutaka Kitamura, Shu-Hong Li, Kenji Ogasawara. Design of a cryogenic CO2 capture system based on Stirling coolers. 2012. International Journal of Greenhouse Gas Control 7 (107-114).
64 ANSYS FLUENT Theory Guide. 2014.
65 ANSYS FLUENT User's Guide. 2014.
66 Mustapha Azreg-Ainou. Low-temperature Data for Carbon Dioxide. 2005. Monatshefte fur Chemie 136, 2017–2027
67 Giauque, W. F., Egan, D.C. Carbon Dioxide. The Heat Capacity and Vapor Pressure of the Solid. The Heat of Sublimation. Thermodynamic and Spectroscopic Values of the Entropy. 1936. Journal of chemical physics 5.
68 Chen, Q.-S., Wegrzyn, J., Prasad, V. Analysis of temperature and pressure changes in liqufied natural gas (LNG) cryogenic tanks. 2004. Cryogenics 44 (701-709).
69 European Standard EN 14620-1. Design and manufacture of site built, vertical, cylindrical, flat-bottomed steel tanks for the storage of refrigerated, liquefied gases with operating temperatures between 0°C and -165°C Part 1: General
70 Na Zhanga, Noam Lior. A novel near-zero CO2 emission thermal cycle with LNG cryogenic exergy utilization. 2006. Energy 31 (1666-1679).
71 Tagliafico, G., Valsuani, F., Tagliafico, L.A. Liquefied natural gas submerged combustion vaporization facilities: process integration with power conversion units. 2011. Int. J. Energy Res. 37 (80-92).
72 Incropera, F.P., Dewitt, D.P., Bergman, T.L, Lavine, A.S. Fundamentals of Heat and Mass Transfer. 2005. John Wiley & Sons.
73 S.J.Jeon, C.H.Chung, Y.U.Kim, H.S.Kim, N.S.Choi. Basic Design for Large Above-Ground Tank. 2002. Gasex 2002.